nature COMMUNICATIONS

ARTICLE

DOI: 10.1038/s41467-018-03393-8 OPEN

MRN complex-dependent recruitment of ubiquitylated BLM helicase to DSBs negatively regulates DNA repair pathways

Vivek Tripathi[1], Himanshi Agarwal[1], Swati Priya[1], Harish Batra[1], Priyanka Modi[1], Monica Pandey[2], Dhurjhoti Saha[3], Sathees C. Raghavan[2] & Sagar Sengupta[1]

Mutations in BLM in Bloom Syndrome patients predispose them to multiple types of cancers. Here we report that BLM is recruited in a biphasic manner to annotated DSBs. BLM recruitment is dependent on the presence of NBS1, MRE11 and ATM. While ATM activity is essential for BLM recruitment in early phase, it is dispensable in late phase when MRE11 exonuclease activity and RNF8-mediated ubiquitylation of BLM are the key determinants. Interaction between polyubiquitylated BLM and NBS1 is essential for the helicase to be retained at the DSBs. The helicase activity of BLM is required for the recruitment of HR and c-NHEJ factors onto the chromatin in S- and G1-phase, respectively. During the repair phase, BLM inhibits HR in S-phase and c-NHEJ in G1-phase. Consequently, inhibition of helicase activity of BLM enhances the rate of DNA alterations. Thus BLM utilizes its pro- and anti-repair functions to maintain genome stability.

[1] National Institute of Immunology, Aruna Asaf Ali Marg, New Delhi 110067, India. [2] Department of Biochemistry, Indian Institute of Science, Bangalore 560012, India. [3] Institute of Genomics and Integrative Biology, CSIR, Mathura Road, New Delhi 110025, India. Correspondence and requests for materials should be addressed to S.S. (email: sagar@nii.ac.in)

DNA damage response (DDR) is an integrated and choreographed response mounted by the cells to eliminate multiple forms of DNA damage that occur in the form of double-strand breaks (DSBs) and stalled replication forks, thereby allowing the faithful replication of the genome. In contrast to stalled replication forks that are recognized by the ATR/Chk1 axis, DSBs are known to be recognized by MRE11–RAD50–NBS1 (MRN) complex, which recruits ATM and allows its optimal activation. ATM, in turn phosphorylates NBS1 leading to the stabilization of MRN complex and subsequently the sequential accumulation of other DDR proteins, thereby allowing the progression of the DDR (reviewed in ref. [1]).

Mutations in tumor suppressor BLM helicase cause Bloom Syndrome (BS). BS patients are characterized by predisposition to multiple types of cancers[2]. Experiments with replication stress have provided evidence that BLM plays an important role in the recognition and subsequent resolution of this type of DNA damage[3]. BLM is an early responder to the formation of stalled replication forks[4] and is recruited to them after being ubiquitylated at three lysine residues by the two chromatin bound E3 ligases, RNF8 and RNF168[5]. The hierarchical position of BLM during replication stress is well deciphered. ATR- and ATM-dependent recruitment of BLM at these sites ensures subsequent ATM activation and 53BP1 focus formation[6]. BLM is essential for the recruitment of MRN complex and BRCA1 to the stalled replication forks[7,8]. However less is known about how BLM is recruited to another more prevalent, potent, and physiological class of lesions, the DSBs. It is known that BLM is an early responder to DSBs[9].Further chromatin loading of BLM to the IR-induced DSBs depends on the presence of Rap1-interacting factor 1 (RIF1) and RNA helicase DEAD Box 1 (DDX1)[10,11]. ATM-mediated phosphorylation of CtIP also promotes the recruitment of BLM to laser-induced DSBs[12].

Once recruited to the site of damage, BLM is involved in its repair. The multiple mechanisms by which BLM functions during homologous recombination (HR), particularly the requirement of its post-translation modifications, have been well documented[13]. For example, BLM is instrumental in the dissolution of both RAD51 nucleoprotein filaments[14–16] and double Holliday junctions[17]. BLM has also been implicated in the negative regulation of error-prone microhomology-mediated end joining (MMEJ). Hence, in cells lacking BLM, the rate of MMEJ-mediated genomic rearrangements was enhanced, indicating BLM prevents this inaccurate pathway of DSB repair[18–20].

In recent past, site-specific cleavage in the human genome has been achieved by fusing the restriction enzyme AsiSI to a modified estrogen receptor (ER) hormone-binding domain, which only binds to 4-hydroxy tamoxifen (4-OHT), an active metabolite of tamoxifen. This has led to the generation of the U2OS–AsiSI–ER system, which has been used previously to obtain the high-resolution profiling of γH2AX around DSBs in the human genome. It was inferred that γH2AX distribution was dependent on gene transcription[21].

Using this U2OS–AsiSI–ER system we have now deciphered the key determinants essential for the recruitment of BLM to the DSBs. We provide evidence that the recruitment of BLM occurs in a biphasic manner extending from 80 bp from the DSBs to 9 kb from the DSBs. While BLM recruitment does not require on its own helicase activity, it is dependent on the kinase activity of ATM and the exonuclease activity of MRE11. Another key requirement is the interaction of RNF8 ubiquitylated BLM with a second MRN complex member, Nbs1. The retention of BLM at the DSBs coincides with its co-recruitment with HR factors in S-phase and c-NHEJ components in G1-phase. The helicase activity of BLM is critical for the phase-specific recruitment of the repair factors to the DSBs. In this phase, BLM recruitment is independent of ATM kinase activity but still depends on the MRE11 exonuclease activity. Post recruitment during the repair phase, BLM not only inhibits HR in S-phase, but also c-NHEJ in G1-phase. Further c-NHEJ is inhibited in the S-phase as a backup mechanism. Thus BLM both enhances and inhibits multiple repair mechanism in a cell cycle phase-dependent manner and thereby maintains genome integrity.

Results

Recruitment of BLM to DSBs is biphasic in nature. In an effort to understand the mechanism of BLM recruitment at the DSBs, we treated U2OS–AsiSI–ER cells with 4-OHT for different time intervals upto 4 h (details of all treatments in the recruitment phase in Supplementary Figure 1A). The extent of DSBs increased with time as indicated both by the levels of the DDR proteins (γH2AX, NBS1, pSer1981 ATM) and their foci formation (Supplementary Figure 2A, C). Concomitant with other DDR factors, the levels of endogenous BLM also increased after DSB generation as early as 30 min after 4-OHT treatment which became more pronounced after 4 h (Supplementary Figure 2A). BLM colocalized with NBS1, γH2AX, and pSer1981 ATM foci (Fig. 1a, Supplementary Figure 2B), further indicating that BLM is an integral component of the DDR. The colocalization between BLM and γH2AX foci was observed as early as 30 min post-damage induction and increased with time (Supplementary Figure 2C).

To elucidate whether BLM is recruited to annotated DSBs formed after 4-OHT treatment, we carried out chromatin immunoprecipitation (ChIP) with anti-BLM antibody in U2OS–AsiSI–ER cells treated with 4-OHT for 4 h. BLM recruitment to both proximal and distal regions to the DSBs on multiple chromosomes (annotated positions in Supplementary Table 1) was determined by ChIP-qPCR by an anti-BLM antibody that did not detect any BLM recruitment when BLM levels are depleted by the cognate BLM siRNA (Supplementary Figure 2D). DSB induction caused BLM recruitment to all the tested seven DSBs spread across different chromosomes (Fig. 1b, Supplementary Figure 2D, E).

To determine whether BLM recruitment was dependent on the compactness of the chromatin, two histone marks, H3K36me3 (associated with euchromatin) and H3K9me3 (associated with heterochromatin), were analyzed utilizing the ChIP-seq data for U2OS cells from the ENCODE database. Analysis of the chromatin landscape on either side of multiple AsiSi sites (by superimposing the primers used for ChIP-qPCR with the ChIP-seq data) revealed that BLM recruitment occurred irrespective of the compactness of the surrounding chromatin (Supplementary Figure 3).

To determine whether the recruitment of BLM was independent of its own helicase function, BLM ChIP was carried out without or in presence of ML216, a specific inhibitor for BLM helicase activity[22] as validated by the SCE assay (Supplementary Figure 2F, G). Presence of ML216 did not prevent BLM from being recruited to the DSBs (Fig. 1c), indicating other transacting factors regulate its recruitment.

To determine the spacial and temporal recruitment of BLM, U2OS–AsiSI–ER cells were exposed to 4-OHT for different time intervals (0.5–4 h) and the extent of recruitment of BLM was determined at different distances (80 bp to 9 kb) from the DSBs for two randomly picked AsiSI sites (annotated positions in Supplementary Table 2). BLM was recruited to the DSBs in a biphasic manner. The first wave of BLM recruitment to the AsiSI-mediated DSBs occurred within 0.5 h, followed by a pronounced decrease in the extent of recruitment upto 2 h. However, 4 h post-DSB induction again led to a robust BLM recruitment onto the chromatin. Interestingly BLM recruitment occurred to roughly

similar extent irrespective of the distance from the DSBs (Fig. 1d, Supplementary Figure 4A).

The biphasic recruitment of BLM indicates that BLM probably has roles in both the early (i.e., the damage sensing step) and late (i.e., the damage repair phase) phase post-DSB generation. To characterize the early recruitment in more detail, we carried out parallel ChIPs with anti-BLM, anti-NBS1, anti-XRCC4, and anti-RAD51 antibodies after exposing the cells to 0.5 h of 4-OHT treatment. It was observed that after 0.5 h of 4-OHT treatment both BLM and NBS1 are co-recruited to the DSBs. The extent of BLM and NBS1 recruitment was higher than RAD51 and XRCC4. This indicated that at this early time point, the DSBs were

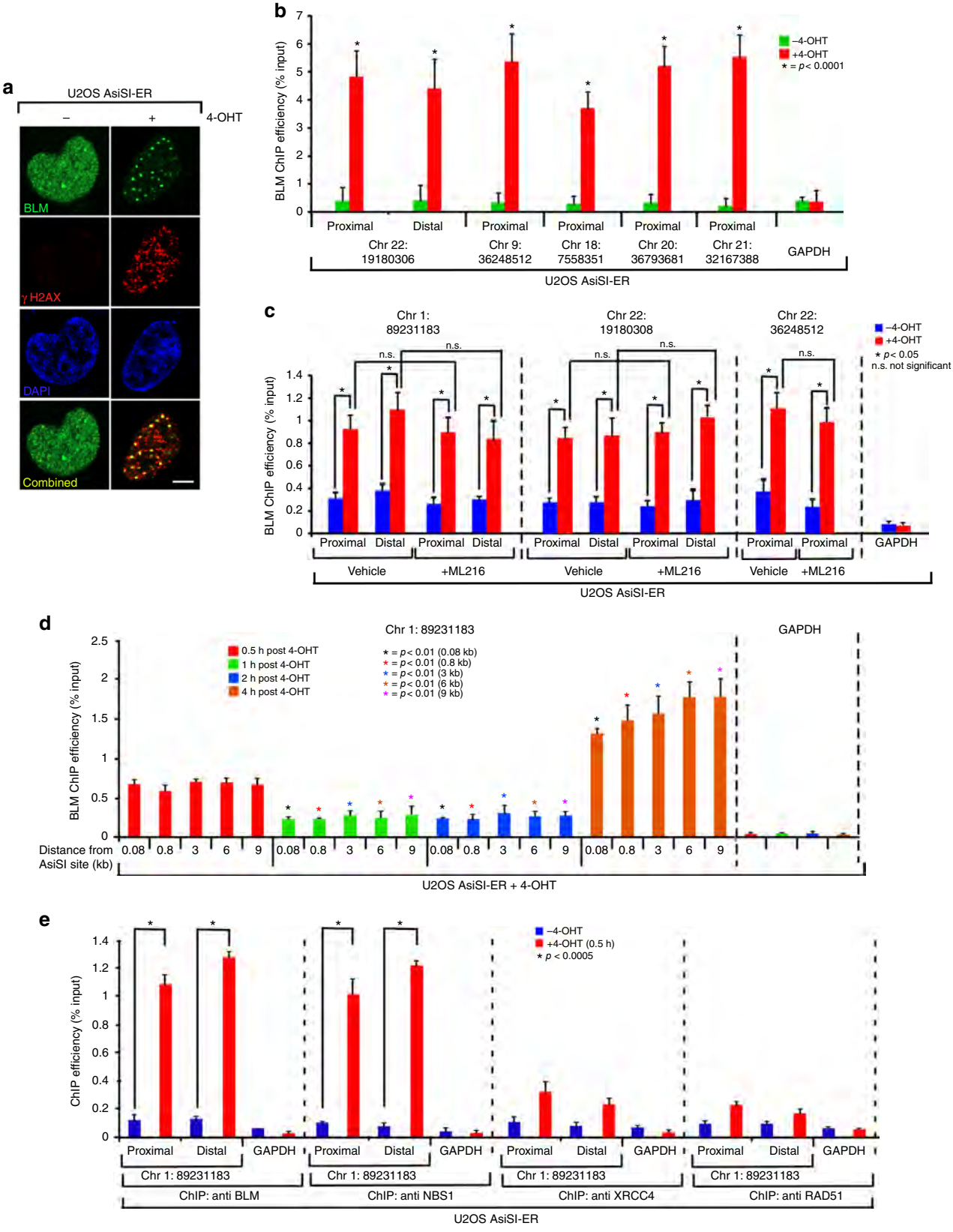

recognized by the DNA damage sensor proteins like NBS1. At this time window, DNA repair processes have not been fully initiated (Fig. 1e, Supplementary Figure 4B).

MRN complex and ATM control BLM recruitment to the DSBs. Since BLM recruitment did not depend on its own helicase activity (Fig. 1c), we wanted to determine the trans-regulatory factors essential for its recruitment to the DSBs. Indeed immunoprecipitations carried out with anti-BLM and anti γH2AX antibodies revealed that co-immunoprecipitation of BLM with pSer1981 ATM, all members of the MRN complex (MRE11, RAD50, and NBS1) and γH2AX (Fig. 2a, Supplementary Figure 5B) increased after 4-OHT treatment in U2OS–AsiSI–ER cells. siRNA mediated depletion of NBS1, MRE11, or ATM (Supplementary Figure 5C, D) abrogated both early (i.e., at 0.5 h) and late (i.e., at 4 h) phase BLM recruitment to both the proximal or distal regions of multiple AsiSI sites after 4-OHT treatment (Fig. 2b, c, Supplementary Figure 6, 7).

Further, to determine whether BLM recruitment at the DSBs depended on the enzymatic activities of MRE11 or ATM, BLM ChIP was carried out after DSB induction, in the absence or presence of either MRE11 exonuclease activity inhibitor (Mirin) or ATM kinase inhibitor (KU 55933). Treatment with either Mirin or KU 55933 prevented the phosphorylation of multiple known ATM substrates (Supplementary Figure 8A, B). In the presence of Mirin, both early (i.e., at 0.5 h) and late (i.e., at 4 h) phase BLM recruitment to all the tested DSBs was decreased by ~50% (Fig. 2d, Supplementary Figure 8C), suggesting that the single-stranded DNA generated by MRE11 exonuclease activity is a key determinant. Interestingly, while the recruitment of BLM in the early phase was dependent on ATM activity, BLM was present on the chromatin even in absence of ATM activity after 4 h of 4-OHT treatment (Fig. 2e, Supplementary Figure 8D). These results indicated that in addition to the physical ablation of the proteins, the loss of exonuclease activity of MRE11 and kinase activity of ATM regulated early BLM recruitment to the DSBs. However, in the second wave of BLM recruitment the requirement of ATM activity is not there indicating the contribution of other factors at this step.

Interaction between BLM and MRN complex in recruitment phase. Based on the present results, we wanted to determine whether MRN-dependent recruitment of BLM after DSB generation also involved its own K63-linked ubiquitylation, as previously shown for replication stress[5]. A low-affinity direct physical interaction between BLM and NBS1 was detected in vitro (Supplementary Figure 9). However, the interaction between RNF8-dependent polyubiquitylated BLM (BLM WT) with immunoprecipitated NBS1 was much stronger compared to non-ubiquitylated BLM (BLM 3K) (Fig. 3a, b, bottom panels). This indicated that BLM polyubiquitylation is the key determinant for its interaction with NBS1. Further in cells lacking BLM, exogenous wild-type BLM but not BLM 3K interacted with endogenous NBS1 (Fig. 3c). Hence lack of BLM polyubiquitylation in vivo (due to depletion of RNF8 by siRNA, Fig. 3d, left), abolished BLM/NBS1 interaction (Fig. 3d, right) in U2OS–AsiSI–ER cells after 4 h of DSB induction. Interaction of polyubiquitylated BLM occurs only with NBS1 and not MRE11 (Fig. 3e). Thus the effect of MRE11 (seen earlier with siMRE11 and Mirin) on BLM recruitment (Fig. 2b, d, Supplementary Figure 6, 8C) is not due to a direct physical interaction. Instead, polyubiquitylated BLM and NBS1 interaction is the key step which brings MRE11 in contact with BLM, allowing BLM to be retained at the DSBs by utilizing MRE11's exonuclease activity.

The above results indicate that ubiquitylation of BLM by RNF8 and the exonuclease activity of MRE11 are possibly two key enzymatic determinants regulating the second wave of BLM recruitment. To test this hypothesis, BLM recruitment to the DSBs was determined in U2OS AsiSI-ER cells after 4 h of 4-OHT treatment by ChIP (Fig. 3f) or foci formation (Fig. 3g, h). The experiment was done in presence of siRNF8 alone, or in cells treated with Mirin or in absence of both RNF8 and the exonuclease activity of MRE11. Lack of either RNF8 (Supplementary Figure 5E) or MRE11 exonuclease activity due to Mirin treatment partially decreased the recruitment of BLM to both the proximal and distal regions of all tested DSBs and partially affected the consequent appearance of the BLM foci. However, depletion of both ubiquitylation and MRE11 exonuclease activities completely abolished BLM recruitment to the DSBs (Fig. 3f–h), suggesting that RNF8-mediated ubiquitylation along with MRE11 exonuclease activity are key events that allows BLM to be recruited to the chromatin.

BLM recruits HR and c-NHEJ factors to chromatin. In an effort to determine the effect of BLM recruitment to the DSBs, we wanted to dissect how BLM affects the two main repair pathways (HR and c-NHEJ) in S- and G1-phase of the cell cycle. ChIPs using BLM, RAD51, and XRCC4 antibodies were carried out in U2OS–AsiSI–ER cells synchronized either in S- or G1-phase of the cell cycle by double thymidine block and subsequently released (Supplementary Figure 10C). The cells in the S- or G1-phase were either left untreated (−4-OHT) or treated with 4-OHT for 4 h. During the S-phase, BLM (Fig. 4a, Supplementary Figure S10B) and RAD51 (Fig. 4b, Supplementary Figure 10C)

Fig. 1 BLM is recruited to AsiSI-induced DSBs. **a** BLM and γH2AX colocalize after DSB induction. U2OS–AsiSI–ER cells were grown asynchronously (−4-OHT) or in the presence of +4-OHT for 4 h. Cells were fixed and stained with anti-BLM and anti-γH2AX antibodies. Nucleus was stained by DAPI. Bar, 5 μM. **b** BLM is recruited to sequence-specific DSBs. U2OS–AsiSI–ER cells were grown asynchronously (−4-OHT) or in the presence of +4-OHT for 4 h. ChIP was carried out using anti-BLM antibody. Recruitment of BLM to the indicated AsiSI-induced DSBs or GAPDH loci were determined by ChIP-qPCR carried out using primers, which were either proximal or distal to the AsiSI sites. **c** Recruitment of BLM to the DSBs is helicase independent. Same as **b**, except BLM recruitment to the indicated AsiSI-induced DSBs was determined in U2OS–AsiSI–ER cells grown either in the absence or presence of ML216. 4-OHT treatment was for 4 h. **d** Biphasic BLM recruitment occurs at both proximal and distal positions with respect to the AsiSI site. Same as **b**, except BLM recruitment to the indicated AsiSI-induced DSB was determined after 4-OHT treatment for 0.5, 1, 2, and 4 h. ChIP was carried out using anti-BLM antibody. Recruitment of BLM to the indicated AsiSI-induced DSBs or GAPDH loci were determined by ChIP-qPCR. Distance from AsiSi site at which recruitment was measured was approximately 0.08, 0.8, 3, 6, and 9 kb. **e** BLM is co-recruited with NBS1 but not with DNA repair proteins to the DSBs in early phase of recruitment. Same as **b** except U2OS–AsiSI–ER cells were treated with 4-OHT for 0.5 h. Parallel ChIPs were carried out with anti-BLM, anti-NBS1, anti-XRCC4, and anti-RAD51 antibodies. Recruitment of BLM, NBS1, XRCC4, and RAD51 to the indicated DSBs or to the GAPDH loci was determined by carrying out ChIP-qPCR analysis. For all ChIP-qPCR analysis, the depicted values (mean ± standard deviation) were obtained from four independent experiments. Data were analyzed by unpaired two-tailed Student's *t*-test

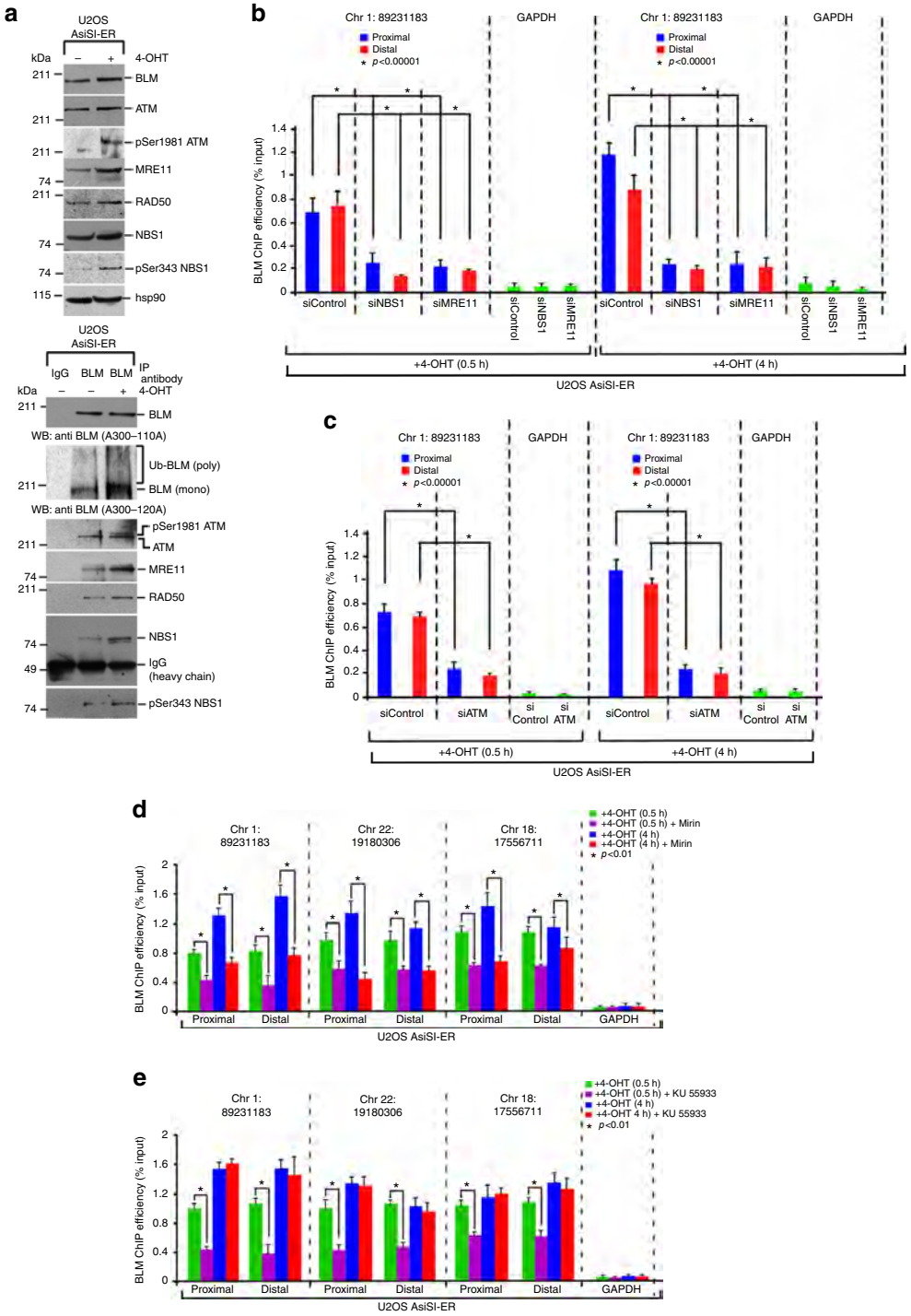

Fig. 2 Recruitment of BLM at the DSBs. **a** BLM co-immunoprecipitates with MRN complex and ATM after DSB generation. (Top) Extracts were made from U2OS-AsiSI-ER cells (±4-OHT, 4 h). Lysates were probed with antibodies against BLM (only A300-110A), ATM, pSer1981 ATM, MRE11, RAD50, NBS1, pSer343 NBS1, hsp90. (Bottom) Immunoprecipitations (±4-OHT, 4 h) were carried out with anti-BLM antibody or the corresponding IgG and the immunoprecipitates were probed with the above-mentioned antibodies. **b**, **c** Recruitment of BLM to the DSBs is dependent on the presence of NBS1, MRE11, and ATM in both 0.5 h and 4 h post induction of DSBs. ChIP was carried out using anti-BLM antibody on chromatin obtained from U2OS-AsiSI-ER cells grown in the presence of 4-OHT for either 0.5 or 4 h after transfection with either **b** Control siRNA or NBS1 siRNA or MRE11 siRNA, or **c** control siRNA or ATM siRNA. BLM recruitment to the indicated AsiSI-induced DSB or GAPDH loci were determined by ChIP-qPCR after either 0.5 or 4 h of 4-OHT treatment. **d** Recruitment of BLM to DSBs partially depends on MRE11 exonuclease activity. ChIP was carried out using anti-BLM antibody on chromatin obtained from U2OS-AsiSI-ER cells grown in presence of 4-OHT for either 0.5 or 4 h. In both the time points, the cells were grown either in +4-OHT or in +4-OHT + Mirin conditions. BLM recruitment to the indicated AsiSI-induced DSBs or GAPDH loci were determined by ChIP-qPCR. **e** Recruitment of BLM to DSBs depends on ATM kinase activity only in the early phase. ChIP was carried out using anti-BLM antibody on chromatin obtained from U2OS-AsiSI-ER cells grown in the presence of 4-OHT for either 0.5 or 4 h. In both the two time points, the cells were grown in +4-OHT or +4-OHT + KU 55933 conditions. BLM recruitment to the indicated AsiSI-induced DSBs or GAPDH loci were determined by ChIP-qPCR. For all ChIP-qPCR analyses, the depicted values (mean ± standard deviation) were obtained from four independent experiments. Data were analyzed by unpaired two-tailed Student's *t*-test

were recruited to both the proximal and distal regions of all the tested DSBs after 4-OHT treatment. In this phase, a low but detectable level of XRCC4 recruitment to the DSBs was also observed (Fig. 4c, Supplementary Figure 10D). Interestingly, BLM was also recruited during G1-phase to the proximal and distal regions of all the DSBs (Fig. 4d, Supplementary Figure 10E) along with XRCC4 (Fig. 4f, Supplementary Figure 10G), but not RAD51 (Fig. 4e, Supplementary Figure 10F). Further, both reciprocal immunoprecipitations and immunofluorescence experiments (Supplementary Figure 11B-E) indicated that BLM interacted with RAD51 during S-phase, while it complexed with XRCC4 in the G1-phase. A minor interaction of BLM with XRCC4 was reproducibly observed in S-phase in both these assays.

We next wanted to determine whether the helicase activity of BLM was essential for the recruitment and retention of the HR and NHEJ factors to the chromatin after induction the DSBs in either G1- or S-phase of the cell cycle. ChIP-qPCR indicated that the absence of BLM helicase activity due to ML216 treatment prevented the optimal recruitment of RAD51 and XRCC4 in S- and G1-phase, respectively (Fig. 4g, h, Supplementary Figure 12). Fractionation studies further indicated that inhibition of BLM helicase activity decreased association of multiple HR factors in S-phase (Fig. 4i) and c-NHEJ factors in G1-phase (Fig. 4j) with the chromatin.

BLM negatively regulates HR and c-NHEJ. Having established the mechanism of BLM recruitment to annotated DSBs (Figs. 1–4), we wanted to determine whether BLM could also specifically regulate the two repair processes at these DSBs in a cell cycle-specific manner. To specifically study the role of BLM helicase

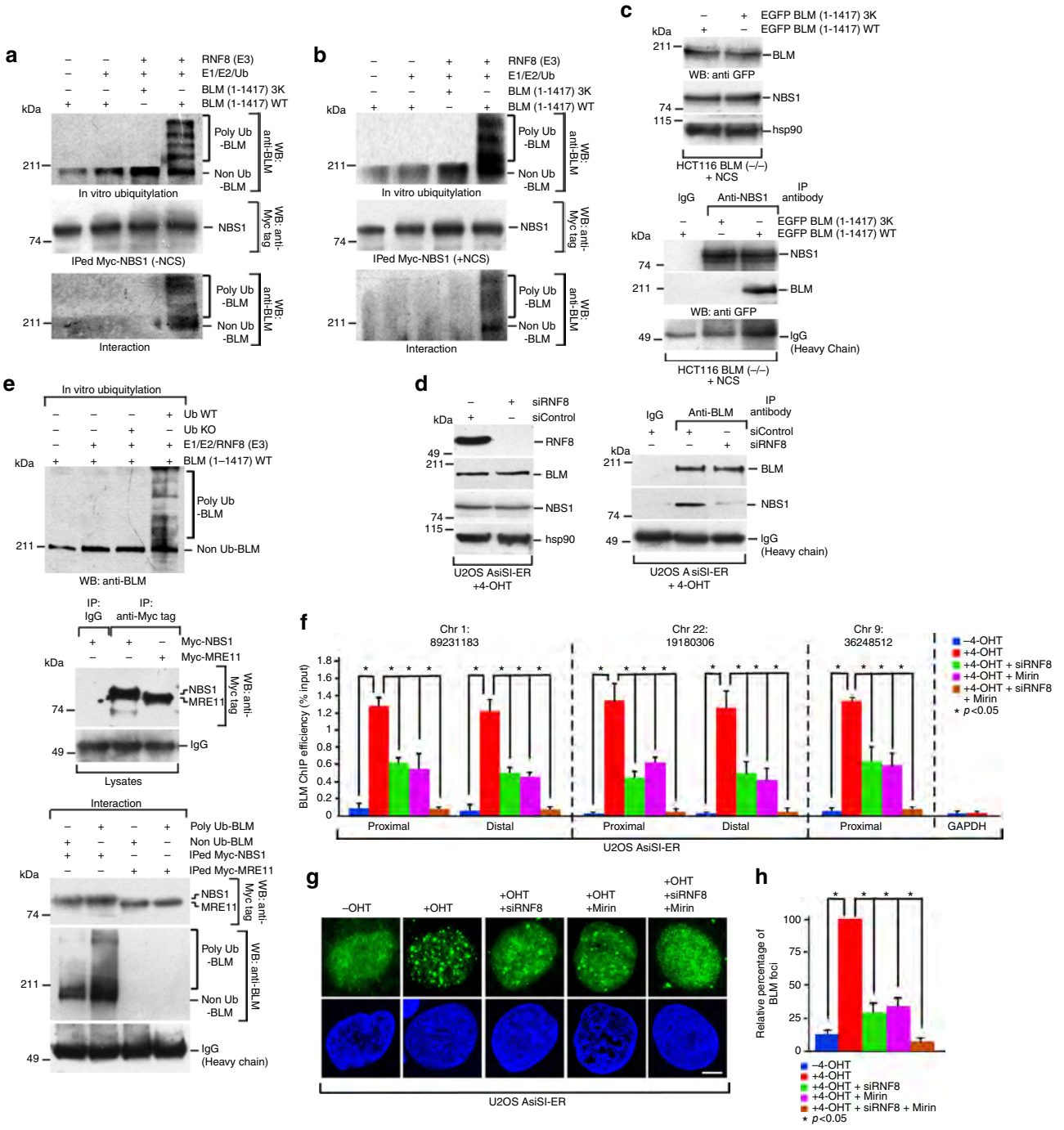

activity during the repair step, DSBs were induced by 4-OHT treatment for 4 h in either S- or G1-phase. Subsequently 4-OHT was washed off and the cell growth was continued for further 1 h (to allow the repair to happen) in absence of 4-OHT but in presence of ML216 or B02 (RAD51 inhibitor that disrupts the binding of RAD51 to DNA)[23] or SCR7 (Ligase IV inhibitor that blocks Ligase IV-mediated end joining by interfering with the DNA binding of Ligase IV)[24] (details of all treatments in the repair phase in Supplementary Figure 1B). During S-phase lack of active RAD51 due to the B02 treatment, decreased the rate of HR to the basal level. Inhibition of BLM activity by ML216 treatment caused an increase in the rate of HR. This negative effect of BLM on HR was not in G1-phase due to the lack of sister chromatids (Fig. 5a). In G1-phase, the major pathway of DNA repair is via NHEJ. Using an intrachromosomal substrate, total NHEJ increased in cells lacking active BLM due to ML216 treatment (Fig. 5b, Supplementary Figure 13A-C). Moreover, ML216 treatment increased the rate of joined product formation, indicating BLM negatively regulated c-NHEJ in G1 phase. As expected, treatment of cells with SCR7 abolished c-NHEJ, while the treatment with B02 forced the cells in S-phase to forgo HR and instead adapt c-NHEJ as the repair pathway. Interestingly, treatment of ML216 also increased c-NHEJ in S-phase. This indicated that though HR is the pathway preferentially inhibited by BLM, it (i.e., BLM) also exerts its negative regulatory effect on c-NHEJ during S-phase (Fig. 5c, d). The presence of both ML216 and SCR7 completely abrogated c-NHEJ in G1-phase, further validating that BLM negatively regulates c-NHEJ (Supplementary Figure 13D, E).

To conclusively demonstrate BLM's role in c-NHEJ, genomic DNA was isolated from G1-phase cells treated with either 4-OHT alone or a combination of 4-OHT and ML216. For either condition, 140 individual clones (35 each from four different AsiSI sites) were sequenced and the extent of different types of nucleotide changes quantitated (Fig. 5e, Supplementary Table 3). Absence of BLM helicase activity statistically increased the rates of sequence alterations (involving deletions, insertions, and deletions with insertions) at or near the AsiSI junctions, thereby providing further evidence that the absence of the helicase activity of BLM negatively affects c-NHEJ in G1-phase.

Discussion

In this report, we delineate the mechanism of BLM recruitment to annotated DSBs spread throughout the human genome and its subsequent effect on DNA repair at these specific sites (Fig. 6). We provide evidence that BLM gets recruited to the DSBs in a biphasic manner. The distance of BLM recruitment ranges from ~80 bp to 9 kb with respect to the DSBs (Fig. 1d, Supplementary Figure 4A). At the DSBs, BLM is co-recruited with multiple components of the DDR pathway via a temporal and cell cycle phase-specific mechanism (Figs. 1e, 4a–f, Supplementary Figure 4B, 10B-G). BLM accumulates with almost equal efficiency on multiple DSBs located on different chromosomes (Fig. 1b, Supplementary Figure 2D, E). It was also observed that BLM recruitment does not depend on the nature of the surrounding chromatin architecture, as recruitment occurs irrespective of whether repressing or activating histone marks surround the AsiSI sites (Supplementary Figure 3). It will be interesting to compare the above mode of BLM recruitment to the recruitment profile of other DDR factors using the same U2OS-AsiSI–ER system. It has been reported that while γH2AX is depleted at the DSBs, it instead spreads to megabase distances away from the break site[21]. In contrast proteins do get recruited only to the immediate vicinity of the DSBs, such as pSer11981ATM[25] and also proteins involved in HR and NHEJ pathway namely RAD51, XRCC4[26]. Hence BLM recruitment seems to be unique as (a) it is present both in the immediate vicinity and far from the DSBs (Fig. 1b, d, Supplementary Figure 2D, E, 4A), (b) has a biphasic recruitment profile (Fig. 1d, Supplementary Figure 4A), and (c) accumulates irrespective of the chromatin architecture (Supplementary Figure 3).

Based on the above recruitment characteristics, BLM's involvement in DDR seems to occur at two distinct phases. In the early phase, BLM is co-recruited with DNA damage sensor proteins like NBS1, γH2AX, pSer1981 ATM within 0.5 h after induction of DNA damage (Fig. 1a, e, Supplementary Figure 2C, 4B). BLM recruitment in this phase occur irrespective of the chromatin architecture (Supplementary Figure 3) and possibly helps DDR by enhancing the functions of histone chaperones[27] and chromatin remodelers[28]. In the second phase of recruitment (4 h post DSB induction), BLM is present at the DSBs along with DNA repair proteins like XRCC4 and RAD51 (Fig. 4a–f, Supplementary Figure 10B-G, 11). In fact BLM is essential for the recruitment of multiple HR and NHEJ proteins to the chromatin (Fig. 4g–j, Supplementary Figure 12), thereby acting as a pro-repair protein. Once recruited, during the repair phase BLM negatively regulates both HR and c-NHEJ (Fig. 5, Supplementary Figure 13, Supplementary Table 3), thereby acting as an anti-repair protein. This dual functions of BLM, as both pro- and anti-repair factor, had been hypothesized earlier based on in vitro experiments[14]. We now provide evidence that these two activities of BLM indeed occur in vivo at two distinct stages in response to DNA damage.

Fig. 3 Ubiquitylated BLM at the DSBs interacts with NBS1. **a**, **b** RNF8-dependent polyubiquitylation of BLM is required for its interaction with NBS1. (Top) **a**, **b** In vitro ubiquitylated BLM WT or BLM 3K was probed with anti-BLM antibody. (Middle) **a**, **b** Exogenous NBS1, immunoprecipitated from HEK293T cells (±NCS), was probed with anti-Myc tag antibody. (Bottom) **a**, **b** Interaction carried out with either polyubiquitylated or non-ubiquitylated BLM and bound Myc-tagged NBS1 was detected with anti-BLM antibody. **c** Ubiquitylation is essential for BLM to interact with NBS1 in vivo. HCT116 BLM (−/−) cells (+NCS) were transfected with either EGFP-C1 BLM (WT) or (3K). (Top) Lysates were probed with antibodies against GFP, NBS1, hsp90. (Bottom) Lysates were immunoprecipitated with antibody against NBS1 and probed with anti-NBS1 and anti-GFP antibodies. **d** Lack of RNF8 prevents the interaction between BLM and NBS1. (Left) U2OS-AsiSi-ER cells were transfected with siControl or siRNF8. Extracts were probed with anti-RNF8, anti-BLM, anti-NBS1, anti-hsp90 antibodies. (Right) Immunoprecipitations, carried out with either anti-BLM antibody or IgG, were probed with anti-BLM, anti-NBS1 antibodies. **e** Polyubiquitylated BLM is complexed with NBS1 but not MRE11. (Top) RNF8-dependent in vitro ubiquitylation of BLM WT, in the presence of Ub WT or Ub with all lysines mutated (Ub KO), was detected using anti-BLM antibody. (Middle) Exogenous Myc-tagged NBS1 and MRE11 were immunoprecipitated and detected with anti-Myc tag antibody. (Bottom) Interactions were carried out with either ubiquitylated or non-ubiquitylated BLM with immunoprecipitated Myc-tagged NBS1 or MRE11 and detected with anti-BLM antibody. **f** Recruitment of BLM to DSBs is abrogated in the presence of Mirin and siRNF8. ChIP was carried out using anti-BLM antibody on chromatin obtained from U2OS AsiSI-ER cells (4 h, 4-OHT). BLM recruitment to the indicated AsiSI-induced DSBs or GAPDH loci were determined by ChIP-qPCR. **g**, **h** Formation of BLM foci are abrogated in presence of Mirin and siRNF8. Experiments were done in same conditions as in **f**. **g** Immunofluorescence was carried out with anti-BLM antibody. Nucleus was stained with DAPI. Bar, 5 μM. **h** Quantitation of BLM foci formed under different conditions. Data were analyzed by unpaired two-tailed Student's *t*-test. Values mean ± standard deviation

The molecular basis that causes this switch in BLM function is yet unknown.

The recruitment of BLM to the DSBs depends on multiple *cis*- and *trans*-factors. *Cis*-factor like the helicase activity of BLM is not essential for its recruitment (Fig. 1c). *Trans*-factors like the physical presence of the MRN complex (specifically NBS1 and MRE11) and ATM protein are the essential prerequisites for the recruitment process (Fig. 2b, c, Supplementary Figure 6, 7). The exonuclease function of MRE11 is essential for the complete recruitment of BLM in both the early and late phase after DSB induction (Fig. 2d, Supplementary Figure 8C). It has been earlier reported that BLM and MRE11 are both part of two end resection complexes that are involved in DNA break repair[29]. Thus the dependence of BLM recruitment to the chromatin after DNA damage on MRE11 expands the role of this exonuclease and indicates that BLM and MRN complexes have multiple functional

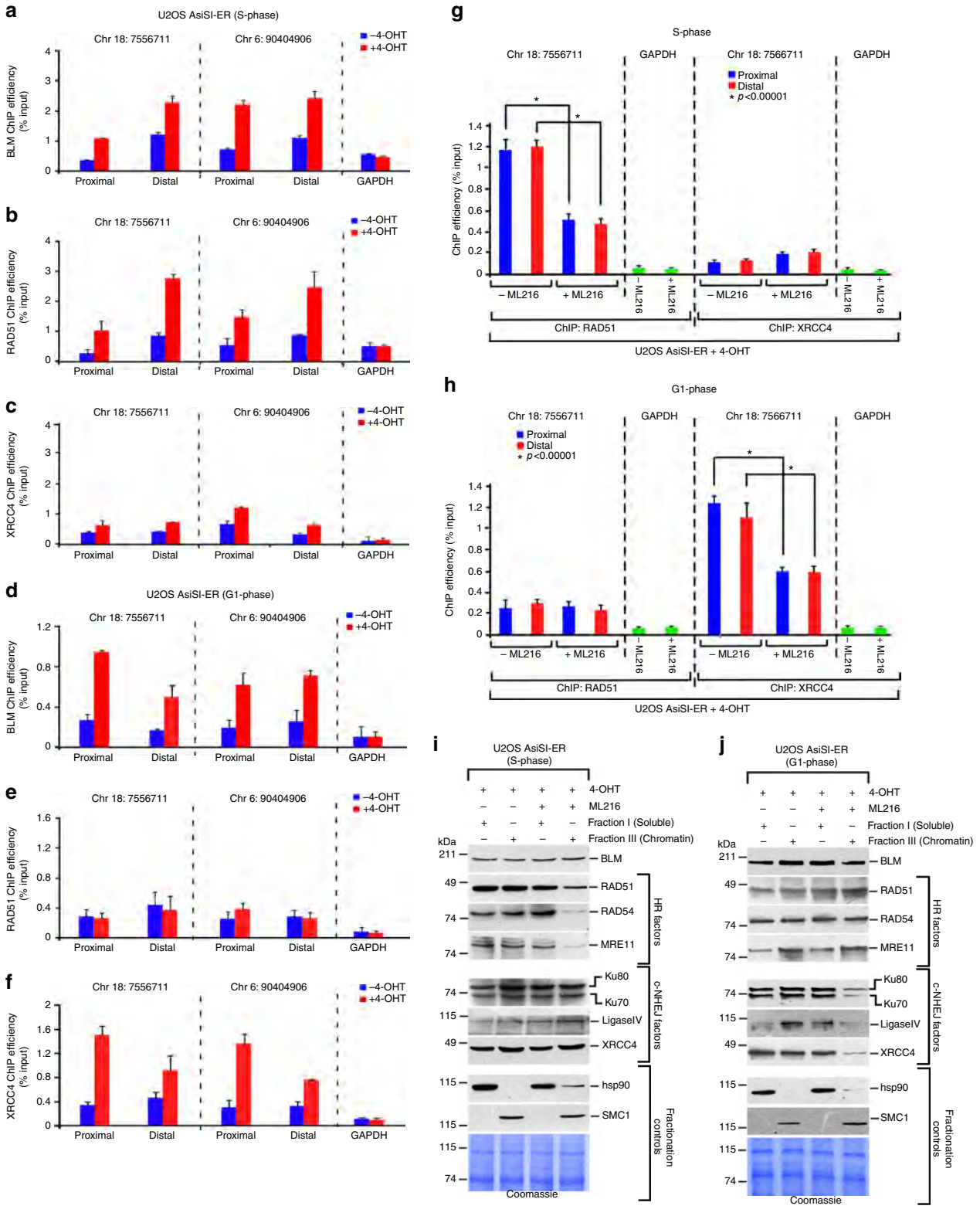

interactions during DNA damage response. In contrast, the recruitment of BLM to the chromatin depends on ATM only in the early phase, i.e., 0.5 h after DSB induction (Fig. 2e), as also observed earlier using laser-induced DSB generating system[12]. BLM dependence on ATM activity maybe direct—as BLM has already been shown to be an ATM substrate[30]. However, it is equally plausible that this is an indirect effect as ATM is known to phosphorylate and thereby regulate the recruitment of both NBS1 and MRE11 onto the chromatin[31]. In the late phase (i.e., 4 h after 4-OHT treatment), the co-recruitment of BLM with DNA repair factors XRCC4 and RAD51 (Fig. 4a–f, Supplementary Figure 10B-G) is independent of ATM kinase activity (Fig. 2e, Supplementary Figure 8D). In this phase, RNF8-mediated BLM ubiquitylation that allows BLM to interact with NBS1, along with the exonuclease activity of MRE11 are the two key essentials for BLM recruitment (Fig. 3f–h).

It is to be noted that while depletion of ATM leads to abrogation of BLM recruitment after both 30 min and 4 h of 4-OHT treatment, inhibition of ATM activity has its effect only at the earlier time point (Fig. 2c, e, Supplementary Figure 7, 8D). This indicates that at the later time periods of DSB induction, BLM that is already at the DSBs do not directly need the kinase activity of ATM. Instead the kinase activity of ATM in this time period is probably needed by its other substrates of the DDR pathway (like MRN complex)[31]. However, the physical presence of ATM is necessary, as without it these other substrates will not get phosphorylated and the DDR pathway cease to be effective. It is interesting to note that though BLM recruitment does not depend on ATM activity after 4 h of 4-OHT treatment, its phosphorylation by ATM at Thr99 might play a role in the repair phase as deciphered from the phenotypes associated with this BLM mutation[30]. Together these results indicate that the interaction of BLM with members of the DDR pathway occurs in both spatial and temporal context.

Interaction between BLM and NBS1 is a key component of BLM recruitment—both being part of the same DDR complex after DNA damage induction (Fig. 2a). Experiments with both endogenous (Fig. 2a) and recombinant proteins (Fig. 3a, b) show that RNF8-mediated BLM polyubiquitylation is a determinant for this interaction. Hence BLM that cannot be polyubiquitylated (either lacking the three lysine residues or in cells where RNF8 is ablated) did not interact with NBS1 in vivo (Fig. 3c, d). Interestingly BLM interaction to MRN complex in vivo is via NBS1 and not MRE11 (Fig. 3e). These results together indicate that in vivo polyubiquitylated BLM's interaction with NBS1 leads to its further association with MRE11, allowing BLM to utilize the latter's exonuclease activity for its own recruitment. This mechanism of BLM recruitment to DSBs is in contrast to the processes characterized for its localization to the stalled replication forks[5], where BLM recruitment predominantly depends RNF8/RNF168-mediated BLM ubiquitylation. Further these BLM ubiquitylation events differ from MIB1 and Fbw7α mediated polyubiquitylation of BLM, both of which lead to BLM degradation by 26S proteasome[32,33].

We have shown that depending on the phase of the cell cycle, BLM is co-recruited with HR and c-NHEJ factors, RAD51 and XRCC4, respectively (Fig. 4a–f, Supplementary Figure 10B-G). Perhaps more importantly BLM is crucial for the optimal recruitment of multiple HR and c-NHEJ factors to the chromatin in a cell cycle-specific manner (Fig. 4g–j, Supplementary Figure 12). The role of BLM in HR regulation has been well studied. BLM and RAD51 physically interact and colocalize at the sites of stalled replication[34–36]. Sumoylation of BLM regulates its interaction with RAD51[37]. We and others have previously shown that BLM disrupts RAD51 nucleoprotein filaments using both cell based and biochemical assays[14–16]. Interestingly we had also reported that the lack of BLM decreased the dynamic mobility and binding of RAD54 and RAD51 to the chromatin[28]. More recently evidence has been provided that BLM can regulate HR by counteracting RAD51 loading at the DSBs[38]. Thus our present data provide further mechanistic insight about how BLM regulates HR in S-phase.

To mechanistically understand how BLM has both a pro-recombinogenic role and also an anti-recombinogenic function, cells were grown in the presence of 4-OHT for 4 h and then for 1 h in media without any 4-OHT (schematic in Supplementary Figure 1B). This 1 h time period was vital as during this period the recruitment phase ceased to exist, the repair phase was initiated at the DSBs and consequently the anti-recombinogenic function of BLM became predominant. Hence while BLM activity was essential for the recruitment of HR and c-NHEJ factors in a cell cycle-specific manner during the recruitment phase (Fig. 4, Supplementary Figure 12), the same BLM activity inhibited HR and c-NHEJ (Fig. 5) in the repair phase due to the switch of BLM from a pro- to anti-recombinogenic role.

Finally, the present work provides evidence that BLM also has a negative regulatory role toward c-NHEJ, both in G1-and in S-phase. Thus in S-phase, BLM not only negative regulates HR but also c-NHEJ, thereby taking care of both the main and backup mechanisms of DNA repair (Fig. 5, Supplementary Figure 13, Supplementary Table 3). The fact that BLM is recruited equally to multiple DSBs irrespective of whether the DSB is in euchromatin or heterochromatin (Fig. 1b, Supplementary Figure 2D, E, 3) and can negatively regulate both HR and c-NHEJ in multiple phases

Fig. 4 Cell cycle-dependent recruitment of HR and c-NHEJ factors is dependent on the helicase activity of BLM. **a**–**c** BLM, RAD51, and XRCC4 are co-recruited to the DSBs in S-phase. U2OS AsiSI were synchronized in S-phase (4 h post release from double thymidine block). Chromatin was prepared from these S-phase cells grown without (−4-OHT) or after 4 h of 4-OHT treatment. ChIP was carried out using **a** anti-BLM antibody; **b** anti-RAD51 antibody; **c** anti-XRCC4 antibody. BLM, RAD51, and XRCC4 recruitment to the indicated AsiSI-induced DSBs were determined by ChIP-qPCR. **d**–**f** BLM and XRCC4 are co-recruited to the DSBs in G1-phase. U2OS-AsiSi-ER cells were synchronized in G1-phase (18 h post release from double thymidine block). Chromatin was prepared from these G1-phase cells grown without (−4-OHT) or after 4 h of 4-OHT treatment. ChIP was carried out using **d** anti-BLM antibody; **e** anti-RAD51 antibody; **f** anti-XRCC4 antibody. Recruitment to the indicated AsiSI-induced DSBs or to the GAPDH loci were determined by ChIP-qPCR. **g**, **h** Helicase function of BLM is required for the cell cycle-dependent recruitment of RAD51 and XRCC4 to the DSBs. U2OS-AsiSI-ER cells were synchronized in either **g** S-phase or **h** G1 phase. Cells in either of the phases were subjected to 4 h of 4-OHT treatment, carried out either in the absence or presence of ML216. Parallel ChIPs were carried out with antibodies against RAD51 and XRCC4. The recruitment of RAD51 and XRCC4 to the indicated AsiSI-induced DSBs or to the GAPDH loci was determined by ChIP-qPCR. For all ChIP-qPCR analyses, the depicted values (mean ± standard deviation) were obtained from four independent experiments. Data were analyzed by unpaired two-tailed Student's *t*-test. **i**, **j** Helicase function of BLM is required for the cell cycle-dependent recruitment of HR and c-NHEJ factors to the chromatin. U2OS-AsiSI-ER cells were grown as in **g**, **h**. Soluble and chromatin fractions were isolated from cells and western analysis carried out with antibodies against BLM, HR factors (RAD51, RAD54, MRE11), c-NHEJ factors (Ku70, Ku80, Ligase IV, XRCC4), fractionation controls (hsp90 for soluble fraction and SMC1 for chromatin fraction). In each case, a Coomassie gel is included to demonstrate that equal amount of protein was taken for the analysis

of the cell cycle (Fig. 5, Supplementary Figure 13, Supplementary Table 3), validates the concept that that DSBs, irrespective of whether they are present in euchromatin or heterochromatin, can employ either c-NHEJ or HR for their repair[39].

In summary, we have determined that ATM, two members of the MRN complex and polyubiquitylation of BLM by RNF8 are the key requirements for BLM recruitment to the DSBs. We have also provided evidence that BLM is the critical upstream component that is required for the recruitment of HR and c-NHEJ factors to the DSBs in a cell cycle-specific manner. We also show that during the repair phase BLM negatively regulates the repair processes, thereby switching from its initial role as a pro-repair protein to an anti-repair protein (Fig. 6). These two functions of BLM are essential to maintain the optimal level of DNA repair in the cells and thereby maintain genome integrity. Recently multiple mechanisms involving post-translation modifications of BLM have been deciphered. These include mechanisms which regulate the constitutive expression of BLM[40], its interaction with TopBP1 and thereby conferring stability[33], its turnover in both mitosis and G1-phase[32,33] and recruitment to PML-NBs[41]. It is quite possible that some these processes that regulate BLM cellular functions may act in close coordination with mechanisms by which BLM responds and ultimately repairs DSBs in different phases of the cell cycle.

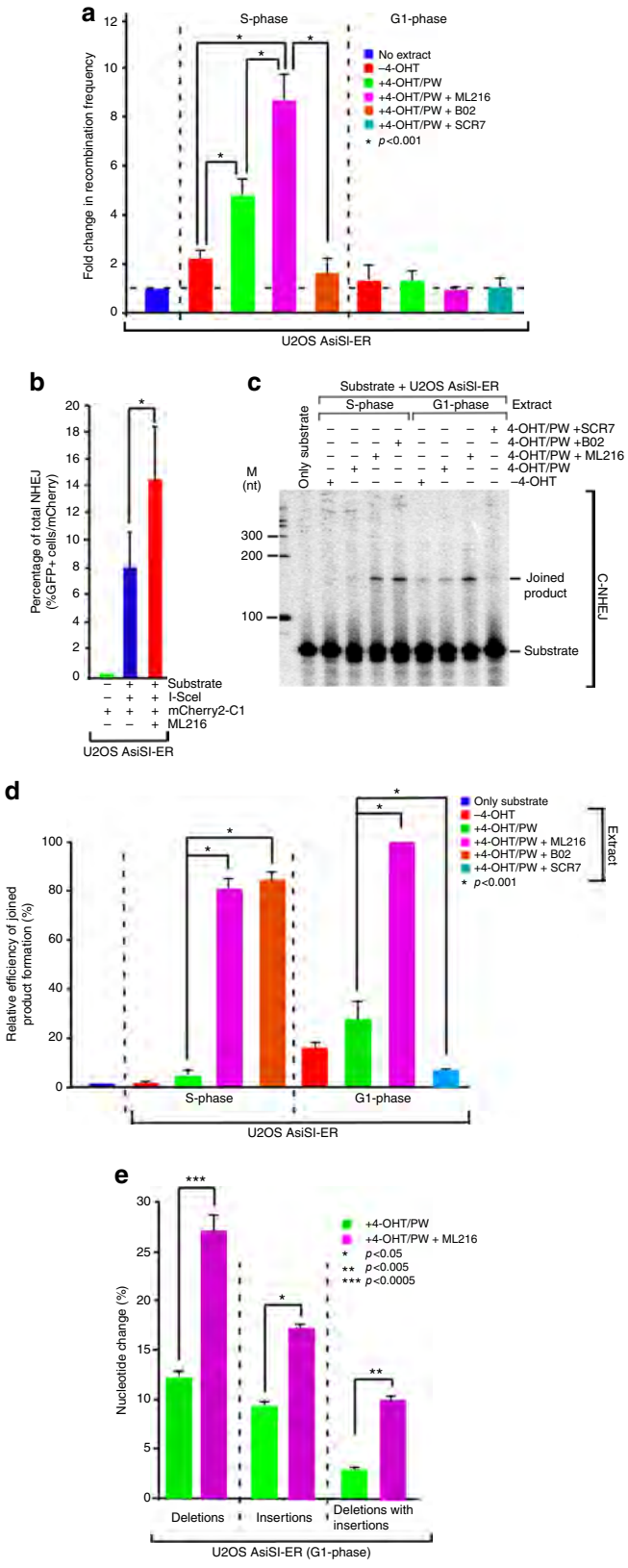

Methods

Reagents. The antibodies used are described in Supplementary Table 4. pcDNA3β myc-NBS1 (a gift of Xiaohua Wu), pcDNA3 myc-MRE11 (a gift of Xiaohua Wu), EGFP-C1 BLM (WT) and EGFP-C1 BLM (3K)[5], pGEX4T-1 BLM (1-1417)[28], mCherry2-C1 (a gift from Michael Davidson, Addgene plasmid #54563), NHEJ substrate pJS296 and I-SceI expression vector pJS20 (gifts from Jemery M. Stark). All siRNAs were purchased from Dharmacon and listed in Supplementary Table 5. Both siRNA transfections (using 200 pmol) and plasmid transfections (in HEK293T) were carried out for 48 h using Lipofectamine 2000 (Thermo Scientific).

Cell culture. U2OS–AsiSi–ER[21] (a gift of Gaelle Legube) and HCT116 BLM (−/−)[42] (a gift of Bert Vogelstein) cells were maintained as described. HEK293T cells were maintained in DMEM medium supplemented with 10% FCS. All cells used were tested free from mycoplasma contamination. Synchronization of U2OS–AsiSi–ER cells in S- and G1-phase by double thymidine block was carried out as published[32]. Supplementary Figure 1 summarizes the growth conditions of U2OS–AsiSI–ER cells used to study the role of BLM in either recruitment phase or

Fig. 5 BLM negatively regulates both HR and c-NHEJ during repair phase. **a** Lack of functional BLM enhances HR in S-phase. HR assays were carried out using extracts from S- or G1-phase-arrested U2OS-AsiSI-ER cells grown in −4-OHT, +4-OHT/PW, +4-OHT/PW + ML216, +4-OHT/PW + B02, +4-OHT/PW + SCR7 conditions. Fold change in recombination frequency is represented with respect to the control where extract was not added. The entire experiment was done three times. Statistical analysis was done by Student's *t*-test. **b** Lack of functional BLM enhances total NHEJ using intrachromosomal substrates. NHEJ substrate (pJS296), I-SceI expression vector (pJS20) and mCherry2-C1 plasmids were co-transfected in asynchronously growing U2OS-AsiSI-ER cells grown in the absence or presence of ML216. The percentage of GFP-expressing cells was scored by FACS analysis. The experiment was done six times, data are presented as mean ± standard deviation and the statistical analysis was done by Student's *t*-test. **c**, **d** Lack of functional BLM enhances c-NHEJ in both S- and G1-phase. c-NHEJ assays were carried out using extracts, which were prepared as in **a**. **c** Representative autoradiogram is shown. **d** Percentage efficiency of joint product formation is represented. The product formed after ML216 treatment in G1-phase is taken as 100% and all other products are calculated relative to the above condition. Data are presented as mean ± standard deviation and the statistical analysis was done by Student's *t*-test. **e** Lack of functional BLM enhances nucleotide change at AsiSI sites. Genomic DNA was isolated from G1-phase-arrested U2OS AsiSI-ER cells grown in +4-OHT/PW, +4-OHT/PW + ML216 conditions. Thirty-five independent clones for each of the four AsiSI junctions were sequenced for both conditions. The percentage of nucleotide changes involving deletions, insertions and deletions with insertions are represented. Data were obtained from three independent experiments and represented as mean ± standard deviation, were analyzed by unpaired two-tailed Student's *t*-test

repair phase. In recruitment phase (Supplementary Figure 1A), U2OS–AsiSi–ER cells were either treated with vehicle (−4-OHT) or treated with 4-OHT (300 nM, Sigma). 4-OHT treatment was for a maximum of 4 h unless otherwise indicated. Cells were treated with Mirin (66 μM, Sigma) and KU55933 (12.9 nM, Sigma) for 1 h prior to and during the 4-OHT treatment. ML216 (12.5 μM, Sigma) treatment was carried out for 24 h prior to and during 4-OHT treatment. B02 (50 μM, Sigma) and SCR7 (66 μM) treatments were carried out during 4-OHT treatment for the last 3 h. For the repair phase (Supplementary Figure 1B), the extracts were made 1 h after 4-OHT was washed off during which the respective drugs used (ML216, B02, SCR7) continued to be present in the medium. Depending on the experiment, cells in −4-OHT conditions were treated with equal volume of the solvent in which ML216, Mirin, KU 55933, B02, or SCR7 were dissolved. Neocarzinostatin (NCS, Sigma, 0.2 ng/μl) treatment of myc-tagged NBS1 and MRE11-transfected cells was for 1 h. The soluble nucleoplasmic (Fraction I) and chromatin bound (Fraction III) components were obtained as described[43]. For cell cycle analysis, the propidium iodide stained DNA content of the cells was sorted in a BD FACS Calibur and analyzed using the FlowJo software.

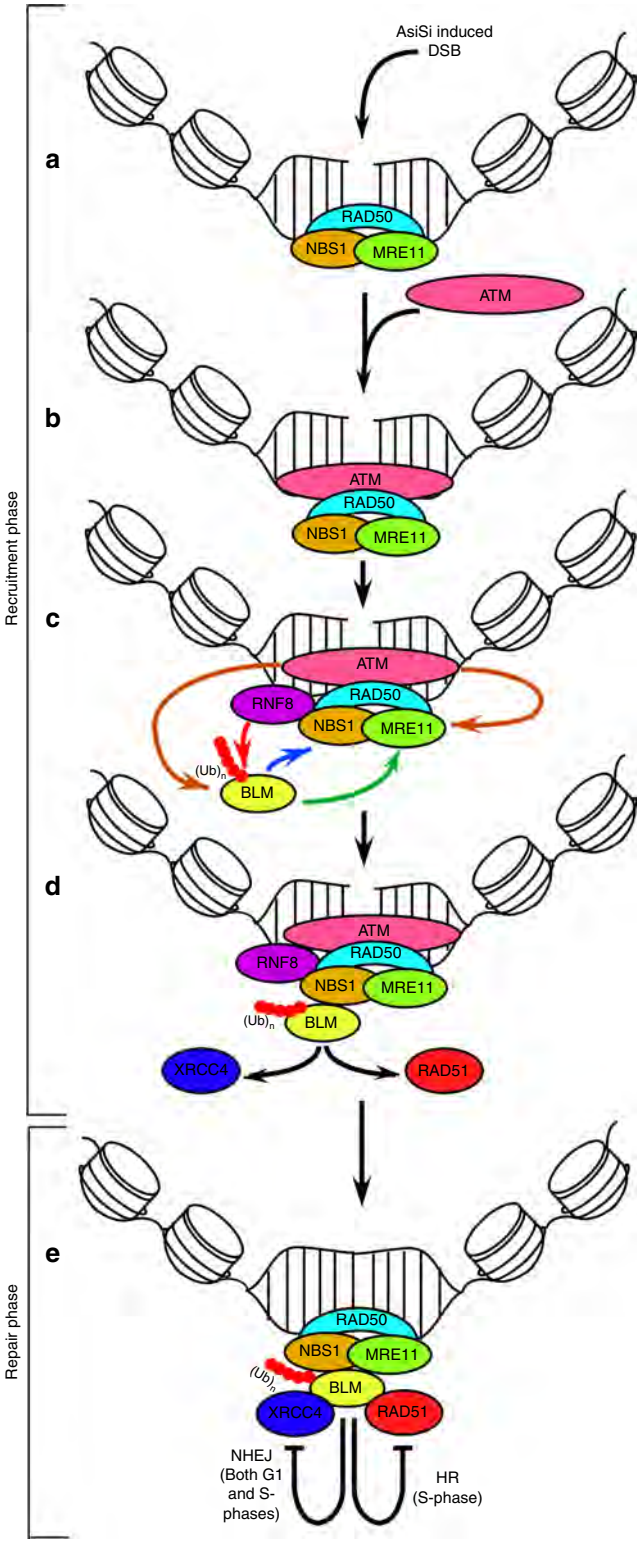

Ubiquitylation, immunoprecipitation and immunofluorescence. RNF8-mediated ubiquitylation of BLM[5] was carried out using 250 ng of the recombinant soluble substrate or 2 μl of in vitro transcribed and translated substrate (Promega). Assays were set up at 37 °C for 3 h in a total volume of 25 μl in 50 mM Tris-HCl (pH 8.0) and 1 mM DTT. Recombinant His-RNF8 (0.2 μM) was added to 0.4 μM of the indicated E2 enzymes Ubc13, 0.0125 μM E1 and 16 μM ubiquitin. Reactions were initiated by the addition of ATP (2 mM) and $MgCl_2$ (5 mM). The reactions were stopped by boiling with 2× SDS loading dye and samples were run on Nu-PAGE 4–12% gels in 1× MOPS buffer (Invitrogen), transferred onto a nitro-cellulose membrane and probed with the indicated antibodies. All lysates were made in RIPA buffer. Myc-tagged NBS1 and MRE11 were immunoprecipitated using 200 μg of RIPA extract and 1 μg of the antibody for 4 h. Interactions between immunoprecipitated myc-tagged NBS1 and MRE11 and BLM were carried out in 1× PBS + 0.1%NP40 buffer overnight at 4 °C. In vivo interactions between endogenous proteins were carried out by standard protocols using 500 μg of lysates and 2 μg of the antibody for 4 h. The protein–protein interactions with ChIP elutes was carried out after extracting the complex twice in elution buffer (0.1 M sodium bicarbonate, 1% SDS) for 15 min at 37 °C. The eluted fractions were pooled and processed for immunoprecipitations, as described above. For in vitro interactions, recombinant GST-BLM or GST (1 μg) was interacted with 5 μl of in vitro translated NBS1 carried out in presence of 20μCi S^{35} methionine. The interaction was carried out at 4 °C for 4 h. Immunofluorescence followed by confocal microscopy was carried out using antibodies and their specific dilutions described in Supplementary Table 4. All incubations with primary antibodies were for 2 hrs while the corresponding secondary antibodies were incubated for 1 hr. Confocal imaging was carried out in LSM510 Meta System (Carl Zeiss, Germany) using 63x/1.4 oil immersion objective. The laser lines used were Argon 458/477/488/514 nm (For FITC) and DPSS 561 nm (for Texas Red). For immunofluorescence quantitation, a minimum of 200 cells across four biological replicates were analyzed. Data presented (mean ± standard deviation) were analyzed by unpaired two-tailed Student's *t*-test.

ChIP assays. ChIP assays using anti-BLM, anti-NBS1, anti-RAD51, and anti-XRCC4 antibodies were carried in U2OS–AsiSi–ER[21]. For this purpose, 250 μg of formaldehyde crosslinked chromatin was immunoprecipitated using 2 μg of the respective antibodies used for all the ChIP assays. After washing, the immunoprecipitated complexes were re-suspended and crosslinking reversed overnight. DNA was purified by phenol/chloroform, precipitated, and analyzed by ChIP-qPCR. Alternatively, ChIP was also carried out using the ChIP assay kit (Millipore, 17-295) as per the manufacturer's protocol. The extent of recruitment of the proteins at the AsiSI-generated cleavage sites was determined by ChIP-qPCR according to the percent input method. All the depicted values (mean ± standard deviation) were obtained from four independent experiments. Data were analyzed by unpaired two-tailed Student's *t*-test. The primers for ChIP-qPCR analysis are described in Supplementary Table 1, 2.

Repair pathway assays and sequencing of AsiSI sites. Lysates for HR and NHEJ assays were prepared[44] in a hypotonic lysis buffer (10 mM This-HCl pH 8, 1 mM EDTA, 5 mM DTT), followed by lysis by homogenization (20 strokes) in presence of protease cocktail inhibitors (Sigma) supplemented with individual

Fig. 6 Mechanism of BLM recruitment to the DSBs and its effect on DNA repair. In the recruitment phase, MRN complex is recruited to the AsiSI-induced DSBs (**a**), which in turn recruits ATM (**b**). Chromatin-bound E3 ligase RNF8 polyubiquitylates BLM (red line, red dots representing ubiquitin residues). The kinase activity of ATM (brown lines) is essential for the BLM recruitment process, acting directly on BLM or via NBS1/MRE11. Single-stranded region obtained due to the exonuclease activity of MRE11 (green line) is also an essential requirement for BLM recruitment. Polyubiquitylated BLM interacts with NBS1 (blue line), which allows BLM to indirectly yet functionally interact with MRE11, leading to the optimal recruitment of BLM (**c**). The helicase activity of BLM is essential for the co-recruitment of c-NHEJ protein XRCC4 in G1-phase and RAD51 in S-phase (black lines) (**d**). During repair phase, BLM predominantly inhibits c-NHEJ in G1-phase and HR in S-phase. As a backup regulatory mechanism, BLM also inhibits c-NHEJ in S-phase (**e**). Hence BLM switches from a pro-repair protein (due to its role in the recruitment phase) to an anti-repair regulatory protein (due to its role in the repair phase), thereby maintaining genomic stability

components. The samples were kept on ice for 20 min, 0.5 volume of high salt buffer (50 mM Tris-HCl, pH 7.5, 1 M KCl, 2 mM EDTA, 2 mM DTT) added. The lysates were ultracentrifuged for 3 h at 211,422.6*g* in a Beckman SW50.1 rotor. Post centrifugation, the sample was dialyzed for 3 h against dialysis buffer (20 mM Tris-HCl, pH 8.0, 0,1 KOAC, 20% glycerol v/v, 0.5 mM EDTA, 1 mM DTT) and frozen in deep freezer. In vitro HR assays were carried[45,46] using (500 ng) of the substrates (pTO231 and pTO223 both of which have ampicillin resistance). Reciprocal recombination and gene conversion between the two substrates lead to the generation of a functional neomycin gene that conferred kanamycin resistance. In the assays, the substrates were incubated with 5 µg of the cell extracts prepared under different conditions. The reaction was carried at 37 °C for 30 min in an HR reaction buffer (35 mM HEPES-pH-8.0, 10 mM $MgCl_2$, 1 mM DTT, 2 mM ATP, 50 µM dNTPs, 1 mM NAD, 100 µg/ml BSA). DNA obtained after Proteinase K treatment, phenol–chloroform extraction, and ethanol precipitation was dissolved in TE buffer and plated in 1:10 ratio between Luria Broth plates containing either ampicillin or kanamycin. Colonies counted after electroporation was used to calculate fold change in recombination frequency. The entire experiment was done three times. Statistical analysis was done by Student's *t*-test. Standard methods of SCE determination were followed[35]. Forty metaphase spreads were analyzed for each condition. Three independent experiments were carried out. The data are presented as mean ± standard deviation and the *p*-values were obtained by Student's *t*-test. The conditions are two-tailed, unpaired data with unequal variance.

NHEJ assays with intrachromosomal substrates were carried out six times[24,47] with certain modifications. NHEJ substrate pJS296 (1 µg) and I-SceI expression vector pJS20 (2 µg) were transfected in asynchronously growing U2OS–AsiSI–ER cells (−4-OHT) in the absence or presence of ML216. mCherry2-C1 plasmid (0.5 µg) was transfected in each case to determine the transfection efficiency. Thirty-six hours post transfection, the cells were collected in PBS and 50 mM EDTA, pelleted and fixed with 2% paraformaldehyde for 20 min. The percentage of mCherry and GFP-expressing cells was scored by FACS analysis in BD FACS AriaIII. The experiment was done six times, data are presented as mean ± standard deviation and the statistical analysis was done by Student's *t*-test. From parallel plates, lysates were made and transfection efficiency was also determined by western blot analysis using an anti I-SceI antibody.

In vitro c-NHEJ assays were carried[24] with [γ-32P] ATP end-labeled double-stranded oligonucleotides containing 5′ compatible ends (top strand: 5′ GAT CCC TCT AGA TAT CGG GCC CTC GAT CCG GTA CTA CTC GAG CCG GCT AGC TTC GAT GCT GCA GTC TAG CCT GAG 3′; bottom strand: 5′ GAT CCT CAG GCT AGA CTG CAG CAT CGA AGC TAG CCG GCT CGA GTA GTA CCG GAT CGA GGG CCC GAT ATC TAG AGG 3′). The data presented are from three biological replicates and are represented as mean ± standard deviation. Data were analyzed by Student's *t*-test.

The genomic DNA around AsiSI sites was cloned in pUC18 and subjected to Sanger sequencing. In both −ML216 and +ML216 condition, 140 individual clones, spanning across four AsiSI sites obtained from three independent experiments were sequenced. Fifty to one hundred nucleotides on both sides of the AsiSI sites were considered to determine the accuracy of the end joining. Data were obtained from three independent experiments and represented as mean ± standard deviation, and were analyzed by unpaired two-tailed Student's *t*-test. The raw sequences from which the data were extracted to determine the nucleotide alterations at or near to the AsiSI sites have been submitted in FigShare: https://figshare.com/articles/Chr6_AsiIS_90404906_pdf/5852853.

Data availability. The individual source files of all the western blots and autoradiograms, presented as TIFF images, are attached as supplementary datasets. The combined source file for all the data are presented in Supplementary Figure 14. Individual source files have been submitted in FigShare: https://figshare.com/articles/Source_File_for_Images/5852940. All other relevant data are available from the authors.

Received: 12 July 2017 Accepted: 9 February 2018
Published online: 09 March 2018

References

1. Ciccia, A. & Elledge, S. J. The DNA damage response: making it safe to play with knives. *Mol. Cell* **40**, 179–204 (2010).
2. Payne, M. & Hickson, I. D. Genomic instability and cancer: lessons from analysis of Bloom's syndrome. *Biochem. Soc. Trans.* **37**, 553–559 (2009).
3. Tikoo, S. & Sengupta, S. Time to bloom. *Genome Integr.* **1**, 14 (2010).
4. Sengupta, S. et al. Functional interaction between BLM helicase and 53BP1 in a Chk1-mediated pathway during S-phase arrest. *J. Cell. Biol.* **166**, 801–813 (2004).
5. Tikoo, S. et al. Ubiquitin-dependent recruitment of the Bloom Syndrome helicase upon replication stress is required to suppress homologous recombination. *EMBO J.* **32**, 1778–1792 (2013).
6. Davalos, A. R., Kaminker, P., Hansen, R. K. & Campisi, J. ATR and ATM-dependent movement of BLM helicase during replication stress ensures optimal ATM activation and 53BP1 focus formation. *Cell Cycle* **3**, 1579–1586 (2004).
7. Davalos, A. R. & Campisi, J. Bloom syndrome cells undergo p53-dependent apoptosis and delayed assembly of BRCA1 and NBS1 repair complexes at stalled replication forks. *J. Cell. Biol.* **162**, 1197–1209 (2003).
8. Franchitto, A. & Pichierri, P. Bloom's syndrome protein is required for correct relocalization of RAD50/MRE11/NBS1 complex after replication fork arrest. *J. Cell. Biol.* **157**, 19–30 (2002).
9. Karmakar, P. et al. BLM is an early responder to DNA double-strand breaks. *Biochem. Biophys. Res. Commun.* **348**, 62–69 (2006).
10. Feng, L., Fong, K. W., Wang, J., Wang, W. & Chen, J. RIF1 counteracts BRCA1-mediated end resection during DNA repair. *J. Biol. Chem.* **288**, 11135–11143 (2013).
11. Li, L. et al. Role for RIF1-interacting partner DDX1 in BLM recruitment to DNA double-strand breaks. *DNA Repair* **55**, 47–63 (2017).
12. Wang, H. et al. The interaction of CtIP and Nbs1 connects CDK and ATM to regulate HR-mediated double-strand break repair. *PLoS Genet.* **9**, e1003277 (2013).
13. Bohm, S. & Bernstein, K. A. The role of post-translational modifications in fine-tuning BLM helicase function during DNA repair. *DNA Repair* **22C**, 123–132 (2014).
14. Bugreev, D. V., Yu, X., Egelman, E. H. & Mazin, A. V. Novel pro- and anti-recombination activities of the Bloom's syndrome helicase. *Genes Dev.* **21**, 3085–3094 (2007).
15. Tripathi, V., Kaur, S. & Sengupta, S. Phosphorylation-dependent interactions of BLM and 53BP1 are required for their anti-recombinogenic roles during homologous recombination. *Carcinogenesis* **29**, 52–61 (2008).
16. Tripathi, V., Nagarjuna, T. & Sengupta, S. BLM helicase-dependent and -independent roles of 53BP1 during replication stress-mediated homologous recombination. *J. Cell. Biol.* **178**, 9–14 (2007).
17. Wu, L. & Hickson, I. D. The Bloom's syndrome helicase suppresses crossing over during homologous recombination. *Nature* **426**, 870–874 (2003).
18. Gaymes, T. J. et al. Increased error-prone non homologous DNA end-joining--a proposed mechanism of chromosomal instability in Bloom's syndrome. *Oncogene* **21**, 2525–2533 (2002).
19. Yamanishi, A. et al. Enhancement of microhomology-mediated genomic rearrangements by transient loss of mouse Bloom syndrome helicase. *Genome Res.* **23**, 1462–1473 (2013).
20. Grabarz, A. et al. A role for BLM in double-strand break repair pathway choice: prevention of CtIP/Mre11-mediated alternative nonhomologous end-joining. *Cell Rep.* **5**, 21–28 (2013).
21. Iacovoni, J. S. et al. High-resolution profiling of gammaH2AX around DNA double strand breaks in the mammalian genome. *EMBO J.* **29**, 1446–1457 (2010).
22. Nguyen, G. H. et al. A small molecule inhibitor of the BLM helicase modulates chromosome stability in human cells. *Chem. Biol.* **20**, 55–62 (2013).
23. Huang, F., Mazina, O. M., Zentner, I. J., Cocklin, S. & Mazin, A. V. Inhibition of homologous recombination in human cells by targeting RAD51 recombinase. *J. Med. Chem.* **55**, 3011–3020 (2012).
24. Srivastava, M. et al. An inhibitor of nonhomologous end-joining abrogates double-strand break repair and impedes cancer progression. *Cell* **151**, 1474–1487 (2012).
25. Caron, P. et al. Non-redundant functions of ATM and DNA-PKcs in response to DNA double-strand breaks. *Cell Rep.* **13**, 1598–1609 (2015).
26. Aymard, F. et al. Transcriptionally active chromatin recruits homologous recombination at DNA double-strand breaks. *Nat. Struct. Mol. Biol.* **21**, 366–374 (2014).
27. Jiao, R. et al. Physical and functional interaction between the Bloom's syndrome gene product and the largest subunit of chromatin assembly factor 1. *Mol. Cell. Biol.* **24**, 4710–4719 (2004).
28. Srivastava, V. et al. BLM helicase stimulates the ATPase and chromatin-remodeling activities of RAD54. *J. Cell. Sci.* **122**, 3093–3103 (2009).
29. Nimonkar, A. V. et al. BLM-DNA2-RPA-MRN and EXO1-BLM-RPA-MRN constitute two DNA end resection machineries for human DNA break repair. *Genes Dev.* **25**, 350–362 (2011).
30. Beamish, H. et al. Functional link between BLM defective in Bloom's syndrome and the ataxia-telangiectasia-mutated protein, ATM. *J. Biol. Chem.* **277**, 30515–30523 (2002).
31. Lavin, M. F., Kozlov, S., Gatei, M. & Kijas, A. W. ATM-dependent phosphorylation of all three members of the MRN complex: from sensor to adaptor. *Biomolecules* **5**, 2877–2902 (2015).
32. Kharat, S. S. et al. Mitotic phosphorylation of Bloom helicase at Thr182 is required for its proteasomal degradation and maintenance of chromosomal stability. *Oncogene* **35**, 1025–1038 (2016).
33. Wang, J., Chen, J. & Gong, Z. TopBP1 controls BLM protein level to maintain genome stability. *Mol. Cell* **52**, 667–678 (2013).

34. Bischof, O. et al. Regulation and localization of the Bloom syndrome protein in response to DNA damage. *J. Cell. Biol.* **153**, 367–380 (2001).
35. Sengupta, S. et al. BLM helicase-dependent transport of p53 to sites of stalled DNA replication forks modulates homologous recombination. *EMBO J.* **22**, 1210–1222 (2003).
36. Wu, L., Davies, S. L., Levitt, N. C. & Hickson, I. D. Potential role for the BLM helicase in recombinational repair via a conserved interaction with RAD51. *J. Biol. Chem.* **276**, 19375–19381 (2001).
37. Ouyang, K. J. et al. SUMO modification regulates BLM and RAD51 interaction at damaged replication forks. *PLoS Biol.* **7**, e1000252 (2009).
38. Patel, D. S., Misenko, S. M., Her, J. & Bunting, S. F. BLM helicase regulates DNA repair by counteracting RAD51 loading at DNA double-strand break sites. *J. Cell. Biol.* doi:10.1083/jcb.201703144 (2017)..
39. Janssen, A. et al. A single double-strand break system reveals repair dynamics and mechanisms in heterochromatin and euchromatin. *Genes Dev.* **30**, 1645–1657 (2016).
40. Kaur, S. et al. Chk1-dependent constitutive phosphorylation of BLM helicase at serine 646 decreases after DNA damage. *Mol. Cancer Res.* **8**, 1234–1247 (2010).
41. Zhu, J. et al. Small ubiquitin-related modifier (SUMO) binding determines substrate recognition and paralog-selective SUMO modification. *J. Biol. Chem.* **283**, 29405–29415 (2008).
42. Traverso, G. et al. Hyper-recombination and genetic instability in BLM-deficient epithelial cells. *Cancer Res.* **63**, 8578–8581 (2003).
43. Lou, Z. et al. MDC1 maintains genomic stability by participating in the amplification of ATM-dependent DNA damage signals. *Mol. Cell.* **21**, 187–200 (2006).
44. Baumann, P. & West, S. C. DNA end-joining catalyzed by human cell-free extracts. *Proc. Natl. Acad. Sci. USA* **95**, 14066–14070 (1998).
45. Oppliger, T., Wurgler, F. E. & Sengstag, C. A plasmid system to monitor gene conversion and reciprocal recombination in vitro. *Mutat. Res.* **291**, 181–192 (1993).
46. Srivastava, N. & Raman, M. J. Homologous recombination-mediated double-strand break repair in mouse testicular extracts and comparison with different germ cell stages. *Cell. Biochem. Funct.* **25**, 75–86 (2007).
47. Bennardo, N., Cheng, A., Huang, N. & Stark, J. M. Alternative-NHEJ is a mechanistically distinct pathway of mammalian chromosome break repair. *PLoS Genet.* **4**, e1000110 (2008).

Acknowledgements

We acknowledge Xiaohua Wu and Jemery M. Stark for plasmids, Gaelle Legube and Bert Vogelstein for cells, and Sumedha Dahal for HR assays, Preeti Attri for FACS analysis, Next Generation Sequencing Facility, NII for help during in silico analysis. S.S. acknowledges the National Institute of Immunology core funds, Indo-French Centre for the Promotion of Advanced Research (IFCPAR) (IFC/4603-A/2011/1250), Council of Scientific and Industrial Research (CSIR) [37(1699)/17/EMR-II], Department of Biotechnology (DBT), India (BT/PR7320/BRB/10/1161/2012 and BT/MED/30/SP11263/2015), and Science and Engineering Research Board (SERB), India (SR/SO/BB-0124/2013) for financial assistance. V.T. acknowledges the Department of Biotechnology for a Research Associate (DBT-RA) position.

Author contributions

V.T., H.A., S.P., H.B., P.M., M.P., and D.S. carried out the experiments and analyzed the data. S.C.R. designed HR, c-NHEJ experiments, and analyzed the data. S.S. designed the overall experiments, analyzed the data, and wrote the manuscript.

Additional information

Supplementary Information accompanies this paper at https://doi.org/10.1038/s41467-018-03393-8.

Competing interests: The authors declare no competing interests.

Reprints and permission information is available online at http://npg.nature.com/reprintsandpermissions/

Publisher's note: Springer Nature remains neutral with regard to jurisdictional claims in published maps and institutional affiliations.

PLOS BIOLOGY

RESEARCH ARTICLE

MITOL-dependent ubiquitylation negatively regulates the entry of PolγA into mitochondria

Mansoor Hussain, Aftab Mohammed☯, Shabnam Saifi☯, Aamir Khan, Ekjot Kaur, Swati Priya, Himanshi Agarwal, Sagar Sengupta*

National Institute of Immunology, Aruna Asaf Ali Marg, New Delhi, India

☯ These authors contributed equally to this work.
* sagar@nii.ac.in

Citation: Hussain M, Mohammed A, Saifi S, Khan A, Kaur E, Priya S, et al. (2021) MITOL-dependent ubiquitylation negatively regulates the entry of PolγA into mitochondria. PLoS Biol 19(3): e3001139. https://doi.org/10.1371/journal.pbio.3001139

Academic Editor: Rong Tian, University of Washington, UNITED STATES

Received: August 21, 2020

Accepted: February 4, 2021

Published: March 3, 2021

Peer Review History: PLOS recognizes the benefits of transparency in the peer review process; therefore, we enable the publication of all of the content of peer review and author responses alongside final, published articles. The editorial history of this article is available here: https://doi.org/10.1371/journal.pbio.3001139

Data Availability Statement: All relevant data are within the paper and its Supporting Information files.

Abstract

Mutations in mitochondrial replicative polymerase PolγA lead to progressive external ophthalmoplegia (PEO). While PolγA is the known central player in mitochondrial DNA (mtDNA) replication, it is unknown whether a regulatory process exists on the mitochondrial outer membrane which controlled its entry into the mitochondria. We now demonstrate that PolγA is ubiquitylated by mitochondrial E3 ligase, MITOL (or MARCH5, RNF153). Ubiquitylation in wild-type (WT) PolγA occurs at Lysine 1060 residue via K6 linkage. Ubiquitylation of PolγA negatively regulates its binding to Tom20 and thereby its mitochondrial entry. While screening different PEO patients for mitochondrial entry, we found that a subset of the PolγA mutants is hyperubiquitylated by MITOL and interact less with Tom20. These PolγA variants cannot enter into mitochondria, instead becomes enriched in the insoluble fraction and undergo enhanced degradation. Hence, mtDNA replication, as observed via BrdU incorporation into the mtDNA, was compromised in these PEO mutants. However, by manipulating their ubiquitylation status by 2 independent techniques, these PEO mutants were reactivated, which allowed the incorporation of BrdU into mtDNA. Thus, regulated entry of non-ubiquitylated PolγA may have beneficial consequences for certain PEO patients.

Introduction

The central factor mediating mitochondrial DNA (mtDNA) replication is the sole catalytic subunit of mtDNA polymerase γ (PolγA). Together with the 2 identical subunits of the processivity factor (PolγB), PolγA forms the functional mtDNA polymerase (PolγA/B2) [1]. Mutations in *POLG*, the gene that codes for PolγA, are associated with mitochondrial disorders like progressive external ophthalmoplegia (PEO), Alpers–Huttenlocher syndrome (AHS), myocerebrohepatopathy spectrum (MCHS) disorders, myoclonic epilepsy myopathy sensory ataxia (MEMSA), and ataxia neuropathy spectrum (ANS). While the mutations in *PolG* are spread over the entire gene body, their frequency is more in the polymerase domain. Most of the common PolγA mutations (like A467T, W748S, and Y955C) have deficiency in catalytic binding and/or polymerase activity as demonstrated by *in vitro* assays [2–4]. It is assumed that mutant

Funding: Sagar Sengupta acknowledges National Institute of Immunology (NII) intramural funding and the following extramural funding sources: Department of Biotechnology (DBT), India (BT/MED/30/SP11263/2015, BT/PR23545/BRB/10/1593/2017, BT/PR27681/GET/119/269/2018), Council of Scientific and Industrial Research (CSIR), India (37(1699)/17/EMR-11), Science & Engineering Research Board (SERB), India (EMR/2017/000541) and J C Bose Fellowship (JCB/2018/000013). EK acknowledges DST Inspire Faculty Fellowship (DST/INSPIRE/04/2017/000088) for salary and funding. Shabnam Saifi acknowledges DBT-RA Fellowship (Batch 35/July 2019/10) for salary and funding. The funders had no role in study design, data collection and analysis, decision to publish, or preparation of the manuscript.

Competing interests: The authors have declared that no competing interests exist.

Abbreviations: AHS, Alpers–Huttenlocher syndrome; ANS, ataxia neuropathy spectrum; CHX, cycloheximide; DTT, dithiothreitol; DUB, deubiquitylating enzyme; IMM, inter-mitochondrial membrane; IPTG, Isopropyl-1-thio-β-D-galactopyranoside; LC1, light chain 1; MAVS, mitochondrial antiviral signaling; MCHS, myocerebrohepatopathy spectrum; MEMSA, myoclonic epilepsy myopathy sensory ataxia; MLS, mitochondrial localization signal; MPP, mitochondrial processing peptide; mtDNA, mitochondrial DNA; NHF, normal human fibroblast; OMM, outer mitochondrial membrane; PEO, progressive external ophthalmoplegia; PMSF, phenylmethylsulfonyl fluoride; PolγA, polymerase γ subunit A; qPCR, quantitative polymerase chain reaction; RT-qPCR, reverse transcription quantitative polymerase chain reaction; TCA, trichloroacetic acid; TIM23, translocase of the inner membrane 23; TOM, translocase of the outer membrane; UPS, ubiquitin proteasomal system; WT, wild-type.

PolγA patient variants also localize into the mitochondrial matrix as the mitochondrial localization signal (MLS) of PolγA is in the extreme N-terminus of the protein [5]. Hence, it is accepted that reductions in the PolγA activity within the mitochondrial matrix cause the dysfunctions associated with the abovementioned mitochondrial disorders. However, it has been reported that low levels of PolγA can also cause inefficient initiation of mitochondrial replication leading to phenotypes associated with PEO [6].

A vast majority of the 1,500 odd proteins which enter mitochondria use the pre-sequences of variable lengths which serve as the targeting motif. These proteins bind sequentially to the translocase of the outer membrane (TOM) complex situated in the outer mitochondrial membrane (OMM) and then to the translocase of the inner membrane 23 (TIM23) complex. Subsequently, the mitochondrial processing peptide (MPP) proteolytically removes the pre-sequences and releases the proteins into the mitochondrial matrix [7]. The intricacy of the regulatory process indicates the mitochondrial outer membrane as a vital regulatory hub for mitochondrial protein import and their subsequent functions.

Ubiquitylation is known to play important roles in multiple functions associated with mitochondria, namely mitochondrial homeostasis, mitochondrial mass, communication of mitochondria with other intracellular organelle, mitochondrial quality control, and mitophagy [8–10]. A variety of proteins involved in different mitochondrial biological processes as diverse as oxidative phosphorylation, Krebs cycle, and mitochondrial dynamics are ubiquitylated [11]. Inhibition of proteasomal degradation results in increased levels of mitochondrial proteins and abnormalities in mitochondrial morphology, thereby indicating to the possibility of uncontrolled protein import leading to the breakdown of the mitochondrial quality control system [12–14]. Hence, it has been hypothesized that when mitochondrial proteins are ubiquitylated, they are mistargeted, thereby compromising the quality of proteins entering the mitochondria [10]. Independent lines of evidences further link the ubiquitin proteasomal system (UPS) and mitochondria: (a) the recruitment of proteasome machinery to the surface of the mitochondria [15,16]; (b) the presence of several components of the ubiquitylation machinery, namely the E3 ligases (MITOL/MARCH5/RNF153; MULAN/MAPL; and PARKIN, RNF185, and KEAP1) and deubiquitylating enzymes or DUBs (USP30 in humans) on the outer membrane of the mitochondria [8]; and (c) the ubiquitylation inhibiting protein import into mitochondria in the yeasts [17].

MITOL/MARCH5/RNF153 (hereafter referred to as MITOL) with 4 membrane spanning segments belongs to RING-CH E3 ligase family. MITOL ubiquitylates, controls the levels, and consequently regulates the functions of a variety of substrates including mitochondrial fission factors like Drp1, Fis1, and MiD49; fusion proteins like Mfn1, Mfn2, and SLC25A46 [10]; and factors which induce mitophagy [18] and neuronal cell death and survival regulatory element, LC1 [19]. MITOL maintains the optimal mitochondrial quality control not only by specifically targeting mutant SOD1 and polyglutamine expanded protein [20,21] but also its own mutant counterpart [22]. Interestingly, MITOL regulates immunopathology during viral infection by targeting mitochondrial antiviral signaling (MAVS) protein and potentiating its degradation [23].

Here, we report that MITOL-mediated ubiquitylation negatively regulated the entry and functioning of PolγA inside the mitochondria. We determined the site on PolγA which was ubiquitylated by MITOL via K6 linkage. Ubiquitylated PolγA could not enter the mitochondria due to its decreased interaction with Tom20. A subset of PolγA mutant proteins expressed in PEO patients was prevented from entering into the mitochondria due to enhanced MITOL-dependent ubiquitylation. Instead, these PolγA variants became enriched in the insoluble fraction and demonstrated enhanced degradation. However, these PEO mutants could be reactivated by inhibiting their ubiquitylation, either by depleting MITOL or mutating the site on

PolγA (K1060) which gets ubiquitylated by MITOL. This allowed the PolγA mutants to enter mitochondria and thereby attain *in vivo* mtDNA replication levels near to that observed for wild-type (WT) PolγA. Overall, our results indicated that MITOL-dependent ubiquitylation act as a negative regulatory mechanism which fine-tuned the entry of PolγA into the mitochondria and thereby controlled its functions.

Results

PolγA levels are decreased by MITOL

Toward an effort to determine the mechanism of turnover PolγA, overexpression of 5 known mitochondrial E3 ligases (MITOL, PARKIN, MULAN, RNF185, and KEAP1) was carried out, and the levels of endogenous PolγA were determined. Only MITOL decreased the levels of PolγA (Fig 1A). MITOL overexpression also decreased the levels of TFAM, but not other proteins involved in mtDNA replication, namely PolγB or Twinkle (Fig 1B). The decrease in the level of PolγA was reversed upon MG132 treatment (Fig 1C) and occurred only in presence of wild-type MITOL (MITOL WT) and not its catalytically dead counterpart (MITOL CD) (Fig 1D). Depletion of MITOL, either transiently by 2 different MITOL siRNAs (Fig 1E) or by the stable expression of shMITOL in HeLa cells [24] (Fig 1F) or in 4-OHT treated MITOL$^{flox/flox}$ MEFs [24] (Fig 1G), all led to increased levels of PolγA and TFAM. However, the levels of other mitochondrial proteins (like Twinkle and Tom20) remained unaffected in absence of MITOL (Fig 1 E–G). The half-life of endogenous PolγA was increased upon depletion of MITOL as revealed by cycloheximide (CHX) chase experiment (Fig 1H and 1I). Importantly, neither the overexpression nor the ablation of MITOL had any effects on PolγA transcript levels (S1A and S1B Fig).

Next, we wanted to determine the binding parameters between PolγA and MITOL. Immunoprecipitation experiments indicated that MITOL interacted with PolγA (Fig 1J). Endogenous PolγA colocalized with endogenous MITOL in hTERT-immortalized normal human fibroblasts (NHFs) (S1C Fig). Similar colocalization was also observed for overexpressed Flag-tagged PolγA with Myc-tagged MITOL (S1D Fig). The spacer and thumb domains in PolγA encompassing amino acids 440–815 [25] (S1E Fig) interacted with MITOL. Reciprocally, the extreme carboxyl terminus cytosol-facing loop in MITOL (amino acids 253–278) interacted with PolγA (S1F Fig).

MITOL ubiquitylates PolγA at K1060 via K6 linkage

Since the level of PolγA is regulated by MITOL, we next wanted to determine whether PolγA is ubiquitylated by this E3 ligase. *In vitro* ubiquitylation indicated that MITOL WT but not MITOL CD ubiquitylated PolγA (Fig 2A). This effect was also recapitulated *in vivo* using overexpressed His-tagged Ub, Flag-tagged PolγA, and Myc-tagged MITOL WT or MITOL CD (Fig 2B). Consequently, the shutdown of MITOL by using its cognate siRNA led to a decrease in the level of ubiquitylation of endogenous PolγA (Fig 2C). Next, we wanted to know the linkage via which MITOL ubiquitylated PolγA. It has been reported that MITOL ubiquitylates its substrates via K48 or K63 linkage [20,23,26]. However, analysis with WT "R" and "O" ubiquitin mutants (described in Materials and methods) indicated that PolγA were ubiquitylated *in vitro* by MITOL via K6 linkage (Fig 2D). We came to this conclusion because except K6R, for none of the other "R" mutants of PolγA, there is a loss of *in vitro* ubiquitylation of PolγA. This indicated that loss of ubiquitylation on PolγA is linked to the lack of lysine residue at K6 position of ubiquitin. Subsequently, when we used the K6O mutant (where only the lysine at sixth position on ubiquitin is present and all other lysines are mutated to alanines) in the *in vitro* ubiquitylation assay, there is a robust ubiquitylation of PolγA. It is to be noted that usage of

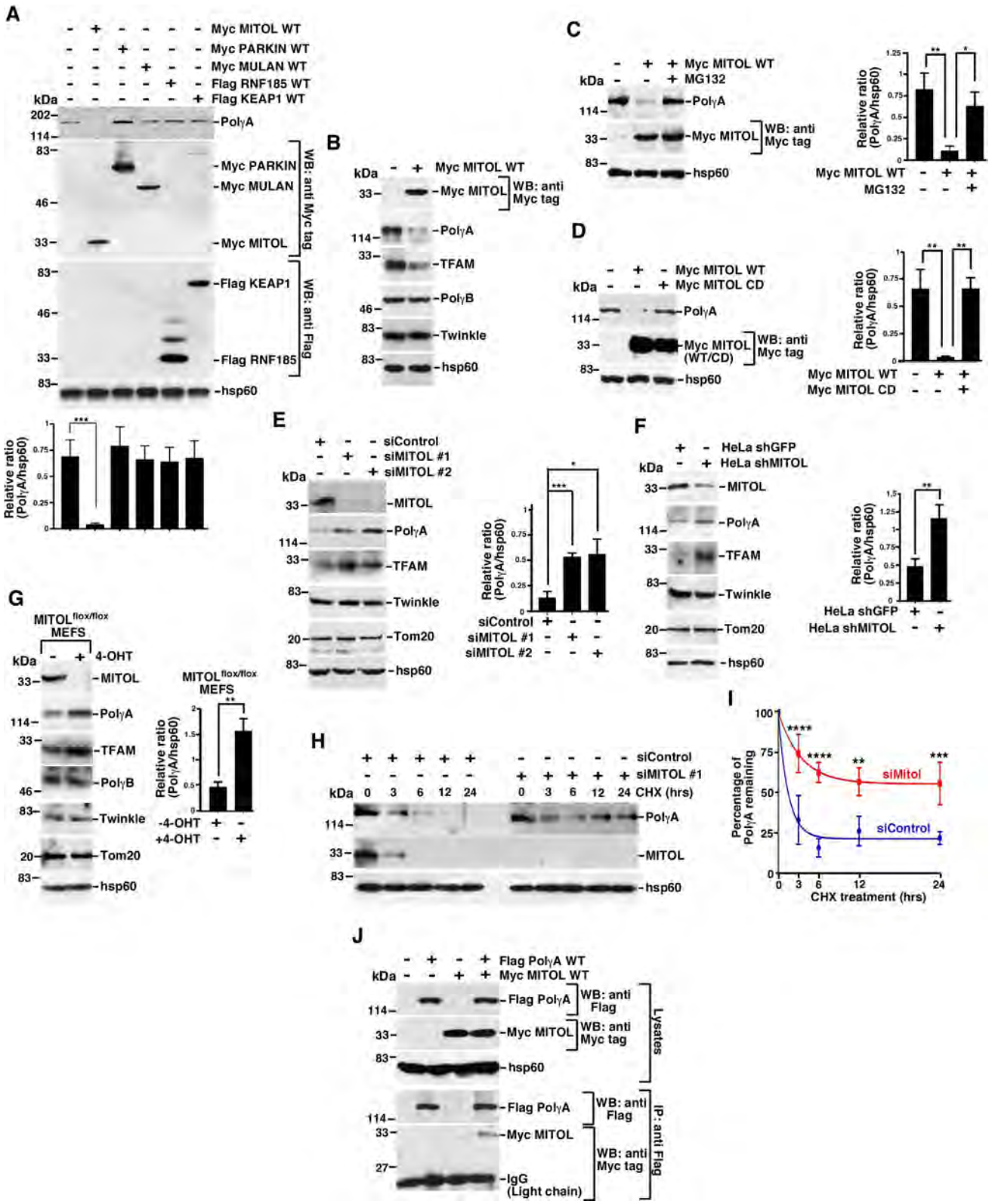

Fig 1. MITOL interacts with PolγA. (A, B) MITOL overexpression leads to decreased levels of PolγA. Whole cell extracts were made from HEK293T overexpressing the indicated mitochondrial E3 ligases. Western blot analysis was carried out with the indicated antibodies. The relative levels of PolγA to hsp60 in (A) have been quantitated from 3 biological replicates. **(C)** MITOL causes proteasomal degradation of PolγA. Whole cell extracts were made

from HEK293T cells overexpressing Myc MITOL for 24 hours and grown either in absence or presence of MG132. Western blot analysis was carried out with the indicated antibodies. The relative levels of PolγA to hsp60 have been quantitated from 3 biological replicates. **(D)** Catalytic activity of MITOL is essential for the proteasomal degradation of PolγA. Whole cell extracts were made from HEK293T cells overexpressing either Myc MITOL WT or CD. Western blot analysis was carried out with the indicated antibodies. The relative levels of PolγA to hsp60 have been quantitated from 3 biological replicates. **(E–G)** Depletion of MITOL stabilizes PolγA. Whole cell extracts were made from (E) HEK 293T cells transfected with either siControl or siMITOL #1 or siMITOL #2 (F) HeLa shGFP and Hela shMITOL cells or from (G) $MITOL^{flox/flox}$ cells either untreated or treated with 4-OHT for 4 days. Western blot analysis was carried out with the indicated antibodies. For all 3 experiments, the relative levels of PolγA to hsp60 have been quantitated from 3 biological replicates. **(H, I)** Half-life of PolγA increases in absence of MITOL. (H) HEK293T cells transfected with either siControl or siMITOL #1. After 24 hours of transfection, cells were grown either without CHX treatment or after CHX treatment for the indicated hours (hrs), and whole cell extracts were made. Western blot analysis was carried out with the indicated antibodies. (I) The percentage of PolγA remaining after CHX treatment has been quantitated. The quantification is from 3 biological replicates. **(J)** PolγA interact with MITOL *in vivo*. (Top) Whole cell extracts were made from HEK293T cells transfected with Flag PolγA and Myc MITOL. Western blot analysis was carried out with the indicated antibodies. (Bottom) Immunoprecipitations were carried out with anti-Flag antibody using the respective lysates. The immunoprecipitates were probed with the indicated antibodies. Three independent biological replicates were carried out, and the same result was obtained. Numerical values for all graphs can be found in S1 Data. See also S1 Fig. CD, catalytically dead; CHX, cycloheximide; IgG, immunoglobulin G; PolγA, polymerase γ subunit A; WT, wild-type.

https://doi.org/10.1371/journal.pbio.3001139.g001

K48O or K63O ubiquitin mutants did not lead to PolγA ubiquitylation, as in these 2 ubiquitin mutants, the lysine at the sixth position in ubiquitin has been mutated to alanine.

Recently, K6- and K33 linkage–specific "affimer" reagents as high-affinity ubiquitin interactors have been characterized [27]. Using K6 linkage–specific affimer, we confirmed that K6 linkage on PolγA also occurred *in vivo* (Fig 2E). Further, we wanted to determine the specificity of MITOL-dependent ubiquitylation on PolγA. We found that the absence of HUWE1, an E3 ligase known to ubiquitylate its substrates via K6 linkage [27], could not increase the level of endogenous PolγA (S2A Fig). This indicated that HUWE1 did not ubiquitylate and thereby degrade PolγA. It has been recently reported that MITOL ubiquitylates multiple mitochondrial proteins, thereby preventing their import [28], while the deubiquitinase USP30 deubiquitylates these substrates, thereby promoting their entry [28,29]. We wanted to test whether USP30 could deubiquitylate MITOL-mediated ubiquitylation on PolγA. Recombinant USP30 (S2B Fig) was added either during (called simultaneous) or after (called sequential) MITOL-mediated *in vitro* ubiquitylation assay. In both the conditions, USP30 could deubiquitylate PolγA (S2C and S2D Fig). However, in asynchronously growing cells, co-expression of USP30 with MITOL could not revert MITOL-mediated decrease in PolγA levels (S2E Fig) nor revert the extent of ubiquitylation on PolγA (S2F Fig). This indicates that there are yet unknown factors or growth conditions which possibly regulate the ubiquitylation–deubiquitylation cycle of PolγA inside the cells.

Next, we wanted to determine the site(s) on PolγA which were ubiquitylated by MITOL. Using a combination of 2 independent ubiquitylation site prediction algorithms (UbPred and UbiPred) and a database (PhosphoSitePlus), a number of lysines were predicted on PolγA which could potentially be ubiquitylated by MITOL. UbPred, UbiPred, and PhosphoSitePlus predicted that PolγA may be potentially ubiquitylated by MITOL on 3 lysine residues. *In vitro* ubiquitylation with lysine to alanine mutants of PolγA indicated that only one of the residues (K1060) was ubiquitylated by MITOL *in vitro* (Fig 2F). This was validated *in vivo* when PolγA K1060R mutant showed complete loss of MITOL-mediated ubiquitylation (Fig 2G). Interestingly, PolγA K1060R interacted with MITOL as well as WT PolγA (Fig 2G), thereby indicating that MITOL could still bind with its substrates in which the site of ubiquitylation had been mutated. This phenomenon, maybe due to an attempted compensatory mechanism of MITOL on PolγA, has also been earlier observed for another MITOL substrate [26].

Ubiquitylated PolγA cannot enter mitochondrial matrix

Having determined that PolγA was ubiquitylated by MITOL, we took the next logical step to understand whether this ubiquitylation affected its entry into the mitochondria. We first used

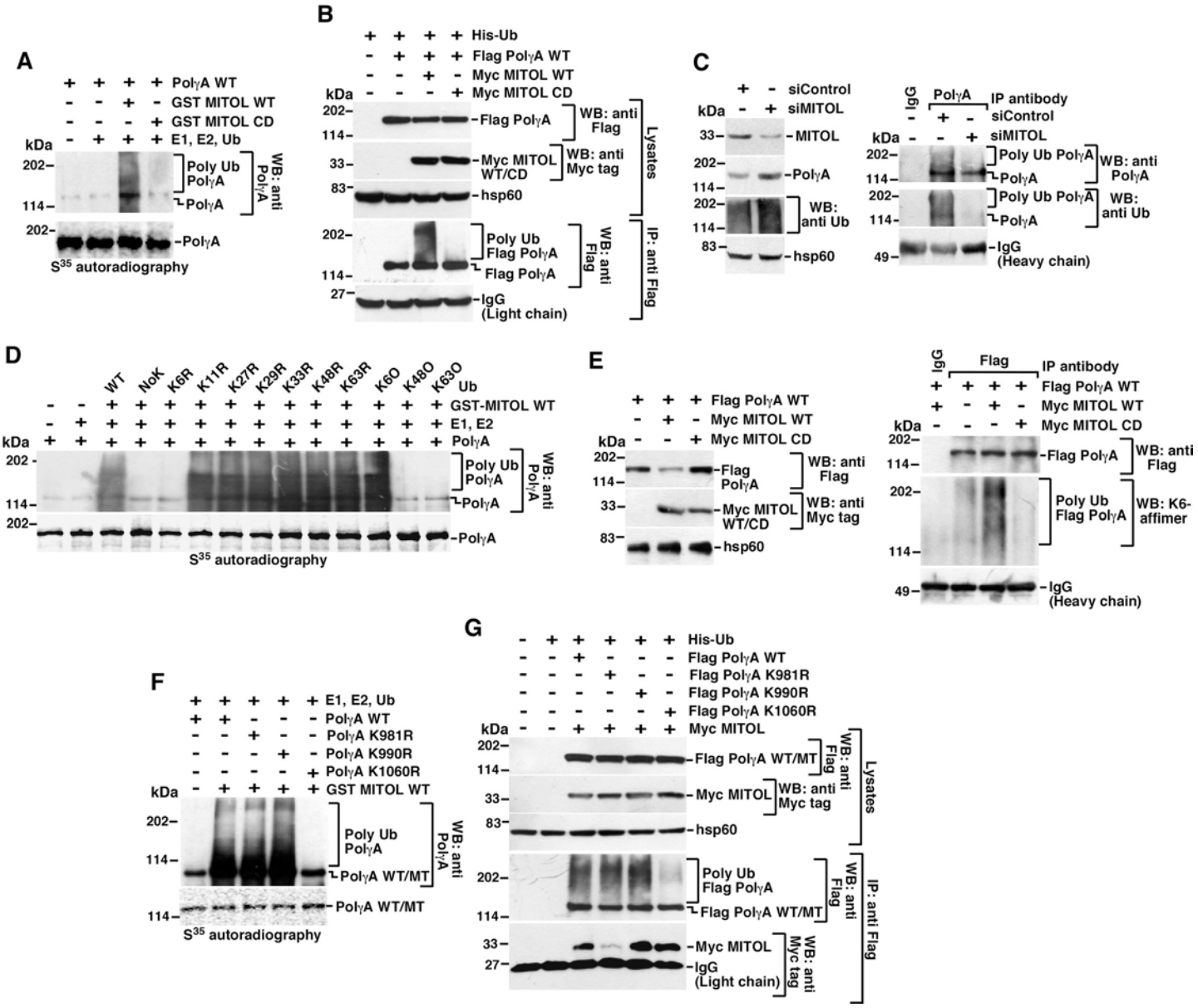

Fig 2. MITOL ubiquitylates PolγA at specific residues via K6 linkage. (A) MITOL ubiquitylates PolγA *in vitro*. *In vitro* ubiquitylation reactions were carried out using PolγA as the substrate and MITOL WT or CD. Post-reaction, the products were detected by western blot analysis with the indicated antibodies. Three biological replicates were carried out, and the same result was obtained. **(B)** MITOL ubiquitylates PolγA *in vivo*. (Top) Whole cell extracts were made from HEK293T cells transfected with His-Ub, Myc MITOL WT, or CD and Flag PolγA. Western blot analysis was carried out with the indicated antibodies. (Bottom) Immunoprecipitations were carried out with anti-Flag antibody, and the immunoprecipitates were probed with the indicated antibodies. Three independent biological replicates were carried out, and the same result was obtained. **(C)** Lack of MITOL prevents PolγA ubiquitylation. (Left) Whole cell extracts were made from HEK293T cells transfected with siControl or siMITOL. Western blot analysis was carried out with the indicated antibodies. (Right) Immunoprecipitations were carried out with anti-PolγA antibody, and the immunoprecipitates were probed with the indicated antibodies. Three independent biological replicates were carried out, and the same result was obtained. **(D)** MITOL ubiquitylates PolγA *in vitro* via K6 linkage. Same as (A), except the indicated "R" or "O" mutants of ubiquitin, were used during the reactions. Three independent biological replicates were carried out, and the same result was obtained. In "R" ubiquitin mutants, only a particular lysine residue in ubiquitin is mutated, while in "O" ubiquitin mutants, only 1 lysine is present on ubiquitin, and all other 6 lysines are mutated. **(E)** MITOL ubiquitylates PolγA *in vivo* via K6 linkage. Whole cell extracts were made from HEK293T cells transfected with MITOL WT or CD in presence of Flag PolγA. (Left) Lysates made were probed with the indicated antibodies. (Right) Immunoprecipitations were carried out with anti-Flag antibody (or the corresponding IgG), and the immunoprecipitates were probed with K6 affimer and the indicated antibodies. Three independent biological replicates were carried out, and the same result was obtained. **(F)** MITOL ubiquitylates PolγA *in vitro* at specific residues. *In vitro* ubiquitylation reactions were carried out using PolγA WT and 3 PolγA mutants, namely PolγA K981R, PolγA K990R, and PolγA K1060R as the substrates. Post-reaction, the products were detected by western blot analysis with anti-PolγA antibody. Three independent biological replicates were carried out, and the same result was obtained. **(G)** MITOL ubiquitylates PolγA *in vivo* at specific residues. (Top) Whole cell extracts were prepared form HEK293T transfected with His-Ub, Myc MITOL, and Flag PolγA WT or PolγA K981R or PolγA K990R, or PolγA K1060R. Western blot analysis were carried out with the indicated antibodies. (Bottom)

Immunoprecipitations were carried out with anti-Flag antibody, and the immunoprecipitates were probed with the indicated antibodies. Three independent biological replicates were carried out, and the same result was obtained. See also S2 Fig. CD, catalytically dead; His-Ub, His-tagged ubiquitin; IgG, immunoglobulin G; PolγA, polymerase γ subunit A; WT, wild-type.

https://doi.org/10.1371/journal.pbio.3001139.g002

both the Flag-tagged and untagged ubiquitylated PolγA and showed that both the versions have equivalent levels of entry into the mitochondrial matrix (Fig 3A and 3B). However, compared to the ubiquitylated variant, non-ubiquitylated PolγA entered the matrix with much better efficiency (Fig 3C and 3D). It was noted that the entry of PolγA did not occur in presence of either CCCP (an uncoupler which dissipated the mitochondrial potential) or Triton X-100 (which solubilized the inner membrane), thereby indicating the authenticity of the entry of PolγA into mitochondrial matrix. To investigate in more detail how ubiquitylation regulated the entry of PolγA, we next carried out an import assay with either PolγA WT or PolγA K1060A (which cannot be ubiquitylated by MITOL, S3A Fig). PolγA K1060R entered mitochondrial matrix with much greater efficiency than PolγA WT (Fig 3E and 3F).

To investigate in more detail how ubiquitylation regulated the entry of PolγA into mitochondria, we carried out ubiquitylation of PolγA for either 5 or 20 minutes (S3B Fig). Mitochondrial import assays for PolγA were carried out with the above reaction products. PolγA which has been ubiquitylated for 5 minutes could enter inside the mitochondria (i.e., the post-trypsin fraction) with much better efficiency (Fig 3G). This indicated a reciprocal relationship between MITOL-dependent ubiquitylation and the mitochondrial entry of PolγA.

Next, we wanted to determine how PolγA ubiquitylation by MITOL affected its entry into the mitochondria. We hypothesized that ubiquitylation of PolγA may negatively affect its binding to Tom20. Ubiquitylated or non-ubiquitylated PolγA were generated by *in vitro* ubiquitylation reactions carried out with either MITOL WT or MITOL CD (S3C Fig). Using these products, *in vitro* interaction experiments were carried out with either GST or GST-Tom20 (S3D Fig). It was revealed that non-ubiquitylated PolγA interacted better with Tom20 (Fig 3H). To further probe whether K6-linked ubiquitylation of PolγA was specifically involved, *in vitro* interaction with GST-Tom20 was carried out with PolγA ubiquitylated by MITOL using either K6R ubiquitin (which does not allow PolγA ubiquitylation, see Fig 2D) or K6O ubiquitin (which allows PolγA ubiquitylation, see Fig 2D). PolγA interacted better with Tom20 when it was generated by using K6R ubiquitin and not when using K6O ubiquitin (Fig 3I, input control in S3E Fig). This indicated that non-ubiquitylated PolγA binds better with Tom20, thereby allowing its better import into the mitochondrial matrix.

PEO mutants have compromised mitochondrial entry and functions

To understand whether the enhanced entry of the non-ubiquitylated PolγA into mitochondrial matrix have any pathological implication, 4 PEO patient mutations were chosen, all of which led to their respective missense mutations (S1 Table). Using *in vitro* transcribed and translated PolγA WT and 4 PEO missense mutants (S4A Fig), it was determined by mitochondrial import assay that PEO mutants #1 and #2 entered mitochondrial matrix with drastically lesser efficiency compared to PolγA WT and the PEO #3 and PEO #4 patient mutants (Fig 4A and 4B, S4B Fig). Using 2.1–2.4-fold overexpressed PolγA WT and patient mutants (S4C Fig), the 2 PEO mutants which could not enter the mitochondrial matrix (i.e., #1 and #2) were found to be ubiquitylated to a higher extent compared to PolγA WT (Fig 4C, bottom panel). In contrast, 2 other PEO mutants (i.e., #3 and #4) were ubiquitylated to a similar extent as PolγA WT (Fig 4C, bottom panel; S4D Fig, right panel). Parallel *in vitro* ubiquitylation reactions with Ub WT and K6O ubiquitin indicated that like PolγA WT, PEO mutants #1 and #2 were also ubiquitylated via K6 linkage (Fig 4D). Consequently, at early time points (see Materials and methods

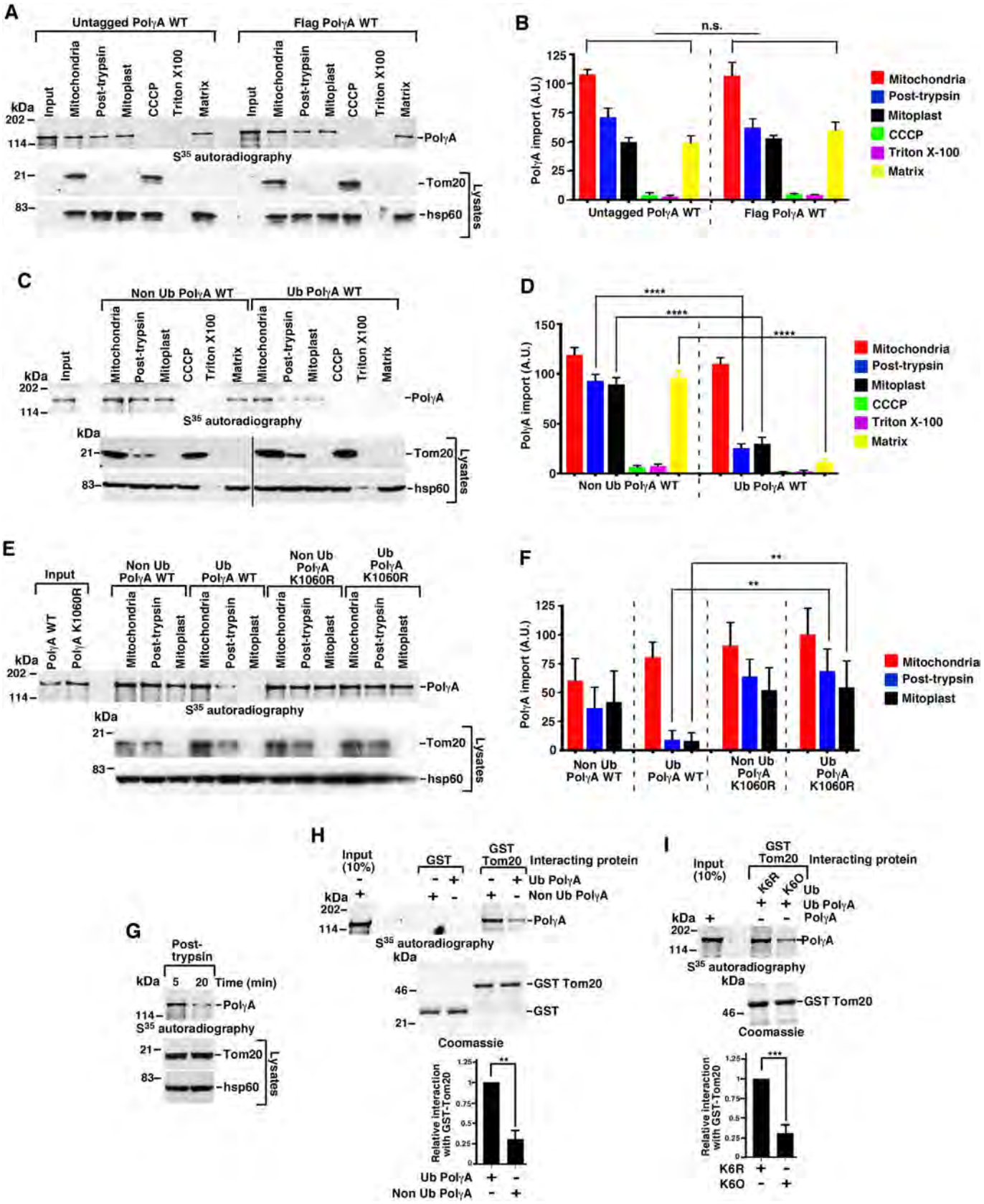
A
Untagged PolγA WT
Flag PolγA WT
Input
Mitochondria
Post-trypsin
Mitoplast
CCCP
Triton X100
Matrix
kDa
202–
114–
21–
83–
PolγA
S35 autoradiography
Tom20
hsp60
Lysates
B
n.s.
PolγA import (A.U.)
125
100
75
50
25
0
Untagged PolγA WT
Flag PolγA WT
Mitochondria
Post-trypsin
Mitoplast
CCCP
Triton X-100
Matrix
C
Non Ub PolγA WT
Ub PolγA WT
D
****
E
Input
PolγA WT
PolγA K1060R
Non Ub PolγA K1060R
Ub PolγA K1060R
F
**
G
Post-trypsin
5
20
Time (min)
H
Input (10%)
GST
GST Tom20
Interacting protein
Ub PolγA
Non Ub PolγA
46–
GST Tom20
GST
Coomassie
Relative interaction with GST-Tom20
I
K6R
K6O
Ub PolγA
***

Fig 3. Ubiquitylation of PolγA negatively regulate its mitochondrial entry. (A, B) Ubiquitylated Flag-tagged and untagged PolγA enters mitochondria with equal efficiency. (A) (Top) Import assays were carried out using the indicated mitochondrial fractions using ubiquitylated S^{35} methionine radiolabeled untagged or Flag-tagged PolγA. The amount of product in each compartment was detected by autoradiography. (Bottom) The integrity of the mitochondria before and after each of the mentioned treatments was determined by carrying out western blot analysis with the indicated antibodies. (B) Quantification of (A), done with data from 3 biological replicates. **(C, D)** Ubiquitylated PolγA enters mitochondria with lesser efficiency. (C) Same as (A) except ubiquitylated or non-ubiquitylated Flag-tagged PolγA was used. (D) Quantification of (C) done with data from 3 biological replicates. **(E, F)** Ubiquitylation site–specific PolγA mutant show enhanced entry into mitochondrial fractions. (E) (Top) Same as (A) except the import assay was carried out with Non Ub Flag-tagged PolγA WT, Ub Flag-tagged PolγA WT, Non Ub Flag-tagged PolγA K1060R, and Ub Flag-tagged PolγA. K1060R. (F) Quantification of (E), done with data from 3 biological replicates. **(G)** Extent of PolγA ubiquitylation determines its mitochondrial entry. Same as (A) except S^{35} methionine radiolabeled PolγA ubiquitylated by MITOL for either 5 minutes or 20 minutes were used as the substrate. The relative import of PolγA in the post-trypsin fraction was determined by autoradiography. The entire experiment was repeated 3 times, and the same results were obtained. **(H)** Non-ubiquitylated PolγA show enhanced interaction with Tom20. Interaction of S^{35} methionine radiolabeled ubiquitylated PolγA (Ub PolγA) and non-ubiquitylated PolγA (Non Ub PolγA) were carried out with either bound GST or GST Tom20. Post-interaction, the bound radioactivity subjected to SDS-PAGE and detected by autoradiography. Coomassie stained gel shows the levels of bound GST or GST Tom20 used in the interactions. The relative interaction of bound GST-Tom20 with Ub PolγA or Non Ub PolγA has been quantitated from 3 biological replicates. **(I)** K6 ubiquitin linked PolγA show decreased interaction with Tom20. Same as (H) except different types of ubiquitin moieties, namely Ub WT, Ub K6R, or Ub K6O were used in the ubiquitylation reactions for PolγA. Coomassie stained gel shows the levels of bound GST Tom20 used in the interactions. The relative interaction of bound GST-Tom20 with Ub PolγA (generated by using either Ub K6R or Ub K6O) has been quantitated from 3 biological replicates. Numerical values for all graphs can be found in S1 Data. See also S3 Fig. PolγA, polymerase γ subunit A; WT, wild-type.

https://doi.org/10.1371/journal.pbio.3001139.g003

for details), PEO patients #1 and #2 were degraded to a larger extent upon MITOL overexpression, an effect which was reversed upon MG132 treatment (Fig 4E). PEO mutants #1 and #2 could not enter mitochondria as they interacted to a greater extent with MITOL but did not bind well with Tom20 receptor on the mitochondrial membrane (Fig 4C, bottom panel). In contrast, PEO mutants #3 and #4 bound to Tom20 with better efficiency (Fig 4C, bottom panel; S3D Fig, right panel). Unlike PolγA WT and PEO mutants #3 and #4, expression of PEO mutants #1 and #2 led to decreased incorporation of BrdU within the mtDNA, as observed both by Southwestern and slot blot western analysis (Fig 4F and 4G). Next, we wanted to compare the above *in vivo* results for PolγA-mediated polymerization with that obtained *in vitro* using the corresponding recombinant proteins (S5A Fig). *In vitro* polymerase activity of all the PEO mutants was greatly diminished compared to PolγA WT (S5B and S5C Fig). *In vitro* exonuclease activity of PEO mutants #1, #2, and #3 was also diminished compared to PolγA WT. However, the exonuclease activity of PEO mutant #4 was comparable to that of PolγA WT (as also reported earlier [30]) (S5D and S5E Fig).

To understand whether suboptimal presence or absence of PolγA within the mitochondria affected the repair efficiency of the mtDNA in the PEO patients, a long-range DNA amplification assay based on quantitative polymerase chain reaction (qPCR) was standardized for the entire 16.2-kb mtDNA. If unrepaired bases in the mtDNA were present, they should terminate the polymerase elongation, thereby decrease the output signal during the PCR reaction. The 110-bp mtND1 PCR product was used to normalize for the amount of mtDNA used for each reaction. Results provided evidence that in contrast to cells expressing PolγA WT, the mtDNA repair ability of PEO mutants #1 and #2 was highly compromised (S6A and S6B Fig).

We further wanted to determine the reason behind the inability of some of the PolγA mutants to enter mitochondrial matrix. Since MITOL is known to prefer aggregated proteins as substrates [20–23], we wanted to know whether PEO mutants #1 and #2 were present in the insoluble cellular fraction compared to PolγA WT and PEO mutants #3 and #4. Again, all the proteins were expressed to equivalent levels (S4C Fig). Cell fractionation indicated that PEO patients #1 and #2 were present to a greater extent in the insoluble fraction compared to their corresponding WT counterparts (S6C and S6D Fig).

Reactivation of PEO mutants

Having demonstrated that PEO mutants #1 and #2 cannot enter mitochondria because of their ubiquitylation by MITOL, we next wanted to determine whether it would be possible to

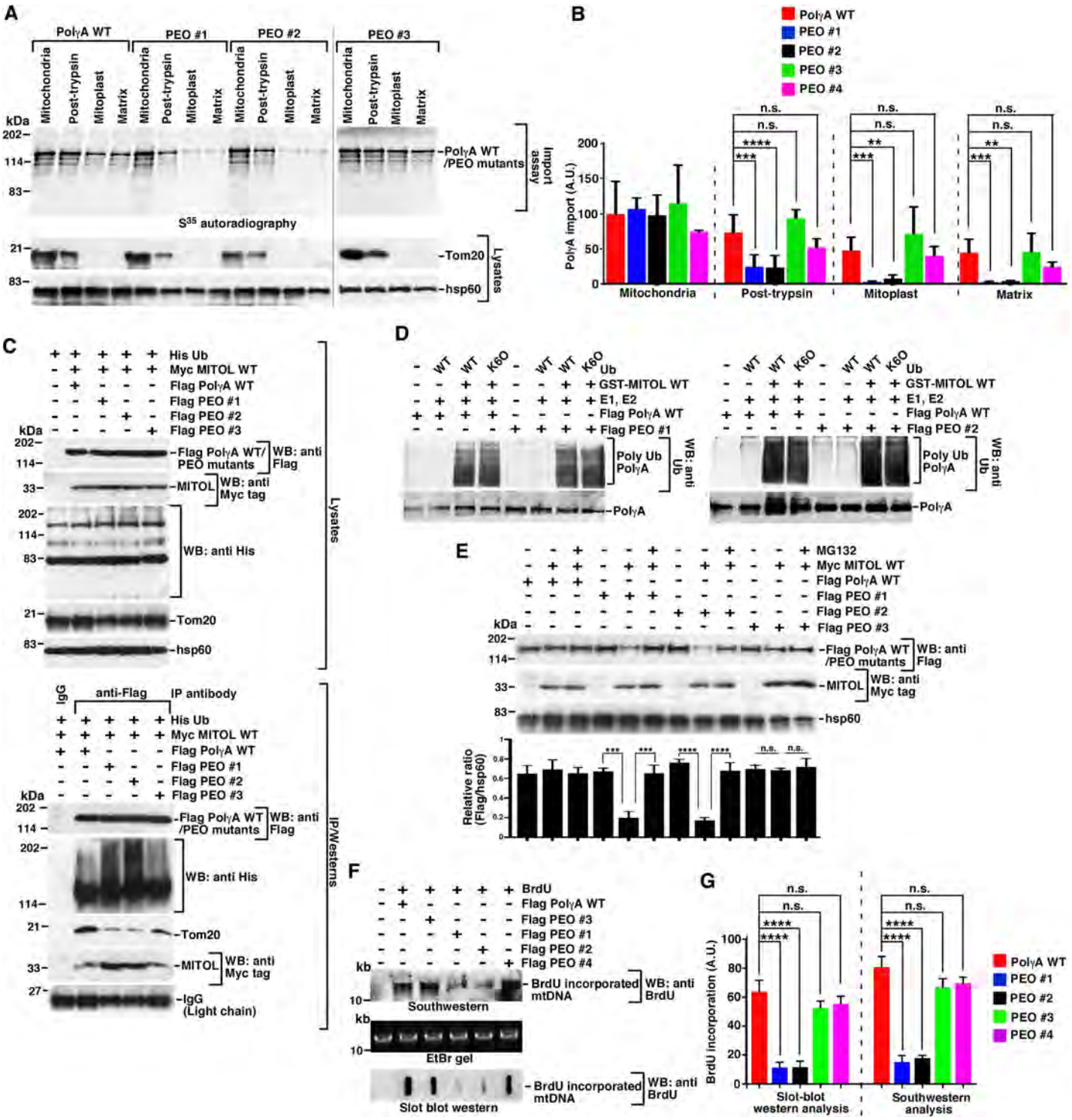

Fig 4. A subset of PEO mutants has compromised mitochondrial entry. (A, B) A subset of PEO mutants has compromised mitochondrial entry. (Top) Mitochondrial import assay was carried out using the indicated mitochondrial fractions. S^{35} methionine radiolabeled PolγA WT, PEO mutant #1, PEO mutant #2, and PEO mutant #3 were incubated with each of the mitochondrial fractions. The amount of product in each compartment was detected by autoradiography. (Bottom) The purity of the mitochondrial fractions was determined using the indicated antibodies. The experiment for PEO mutant #3 was done independently, and separate blots were obtained. (B) Quantification of A and S4B Fig is presented. Data are from 3 biological replicates. **(C)** Subset of PEO patients shows enhanced ubiquitylation and reduced binding to Tom20. (Top) Whole cell extracts were made from HEK293T cells transfected with His-Ub, Myc MITOL WT, Flag PolγA WT, Flag PEO mutant #1, Flag PEO mutant #2, and Flag PEO mutant #3. Western blot analysis was carried out with the indicated antibodies. (Bottom) Immunoprecipitations were carried out with anti-

Flag antibody (or the corresponding IgG), and the immunoprecipitates were probed with the indicated antibodies. Three independent biological replicates were carried out, and the same result was obtained. **(D)** MITOL ubiquitylates PEO mutants *in vitro* via K6 linkage. *In vitro* ubiquitylation reactions were carried out using PolγA, Flag PEO mutant #1, Flag PEO mutant #2 as the substrate, MITOL WT, and ubiquitin (WT or K6O). Post-reaction, the products were detected by western blot analysis with the indicated antibodies. Three biological replicates were carried out, and the same results were obtained in each case. **(E)** Subset of PEO mutants has enhanced rate of proteasomal degradation. Whole cell extracts were made from HEK293T cells overexpressing Myc MITOL WT, Flag PolγA WT, Flag PEO mutant #1, Flag PEO mutant #2, and Flag PEO mutant #3 and grown either in absence or presence of MG132. Western blot analysis was carried out with the indicated antibodies. The relative levels of Flag PolγA variants to hsp60 have been quantitated from 3 biological replicates. **(F, G)** Cells expressing subset of PEO mutants have lesser capability of mtDNA replication. (F) mtDNA replication in HEK293T cells expressing Flag PolγA WT, Flag PEO mutant #1, Flag PEO mutant #2, Flag PEO mutant #3, and Flag PEO mutant #4 were determined either by (top) Southwestern analysis or (bottom) Slot blot western using anti-BrdU antibody. (Middle) An EtBr gel for NheI digestion of mtDNA shows equal amount of DNA taken for both the assays. (G) Quantification of (F) from 3 biological replicates. Numerical values for all graphs can be found in S1 Data. See also S4–S6 Figs. His-Ub, His-tagged ubiquitin; IgG, immunoglobulin G; mtDNA, mitochondrial DNA; PEO, progressive external ophthalmoplegia; PolγA, polymerase γ subunit A; WT, wild-type.

https://doi.org/10.1371/journal.pbio.3001139.g004

reactivate the same PEO mutants. We tested out 2 strategies to reactivate these 2 PolγA mutants that cannot enter mitochondria. In the first strategy, we wanted to check whether upon ablation of MITOL, PolγA mutants #1 and #2 become reactivated. Indeed, ablation of MITOL in HeLa shMITOL cells led to entry of both PEO mutants #1 and #2 into mitoplast (Fig 5A). Next, we wanted to determine the extent of ubiquitylation of these 2 mutants in comparison to PolγA WT in the whole mitochondrial lysates (Fig 5B, left). As expected, the extent of ubiquitylation in PEO mutants #1 and #2 was much higher than PolγA WT in HeLa shGFP cells (Fig 5B, middle). However, in HeLa shMITOL cells, low but equivalent levels of ubiquitylation were observed for all the 3 PolγA variants (Fig 5B, right), indicating that the lack of MITOL was the critical factor for their successful mitochondrial entry into the mitochondria. Both Southwestern and slot blot analysis indicated that HeLa shMITOL cells expressing PolγA WT or PEO mutant #1 or #2 were able to incorporate BrdU to significant levels, thereby indicating successful reactivation for these mutants (Fig 5C and 5D).

However, we recognized that given the importance of MITOL as an E3 ligase and its many of substrates having critical cellular functions [31], inactivating it may not be a viable solution to reactivate PEO mutants. Hence, as a second strategy, we wanted to determine whether it is possible to increase the entry of PEO mutants #1 and #2 into mitochondrial matrix and thereby attain their reactivation. We hypothesized that since PEO mutants #1 and #2 were hyperubiquitylated, changing lysine 1060 residue to arginine (PolγA K1060R) should abolish their ubiquitylation by MITOL and thereby help them to bind to Tom20 and allow them to enter the mitochondrial matrix. Immunoprecipitation experiments revealed that K1060R counterparts of both PEO mutants #1 and #2 were not hyperubiquitylated (Fig 6A, right panel). This allowed PEO mutant #1 K1060R and PEO mutant #2 K1060R to bind as strongly with Tom20 as PolγA WT (Fig 6A, right panel). The K1060R counterparts of the PEO mutants #1 and #2 entered the mitochondria with efficiencies which were significantly more than that observed for PEO mutants #1 and #2 themselves (Fig 6B and 6C). Slot blot western and Southwestern analysis also revealed greater incorporation of BrdU in cells expressing the K1060R versions of mutants #1 and #2 (Fig 6D and 6E), indicating that the lack of mtDNA replication in PEO mutants #1 and #2 can be reverted to an extent, and significant reactivation of these 2 PEO mutants have been achieved. Finally, we wanted to determine whether this reactivation was due to decrease in the accumulation of PEO mutants #1 and #2 K1060R variants in the insoluble fraction. Compared to PEO mutants #1 and #2, their K1060R variant accumulated much less in the insoluble fraction (S6E and S6F Fig), which possibly made them less likely to become MITOL substrates.

Discussion

Studies have been shown that MITOL carries out its function by acting as a multifunctional protein on the OMM. MITOL acts as a key signaling factor which controls the mitochondrial

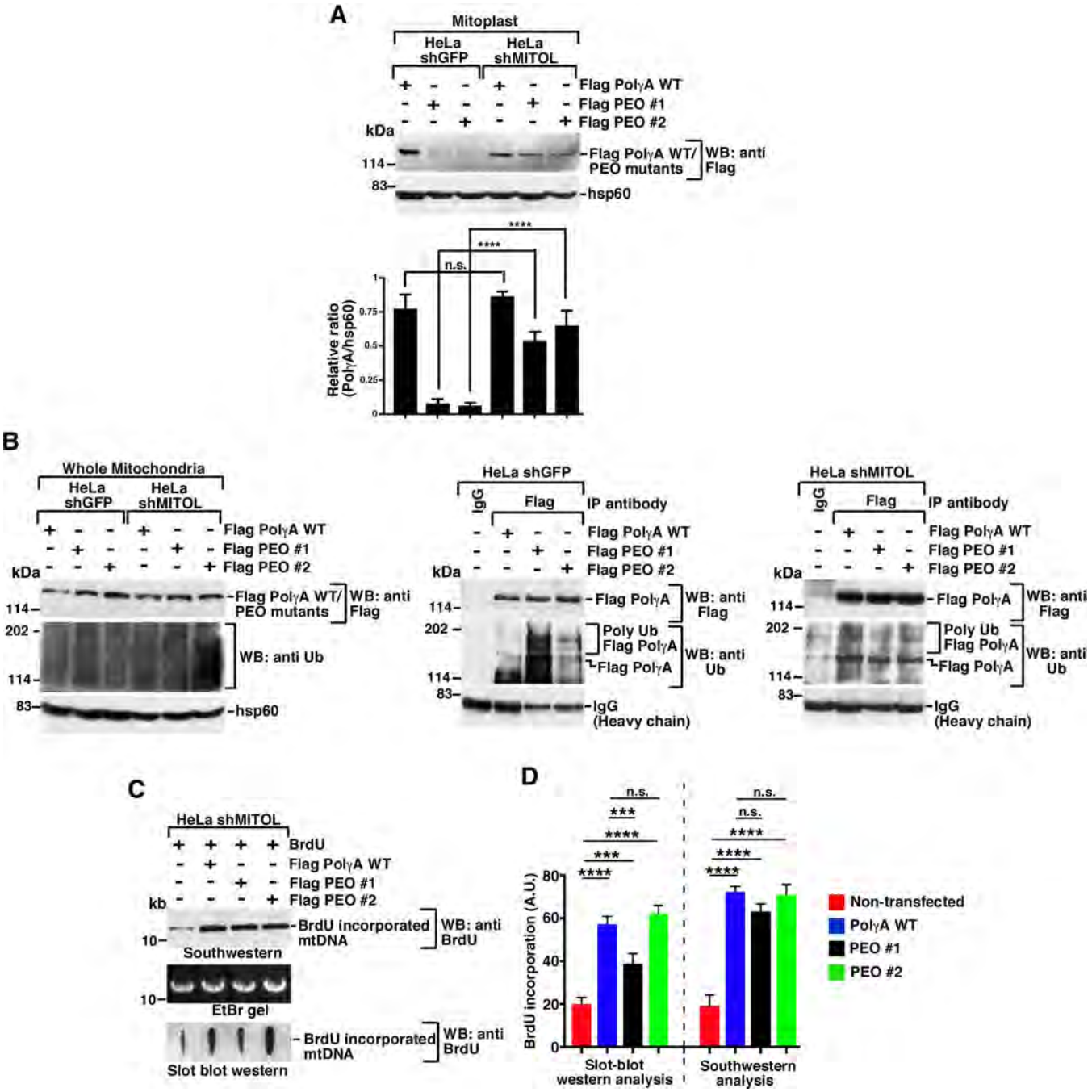

Fig 5. PEO mutants can be reactivated by depleting MITOL. (A) HeLa shMITOL cells show increased entry of PEO mutants. Mitoplasts were isolated from HeLa shGFP and HeLa shMITOL cells expressing Flag PolγA WT, Flag PEO mutant #1, and Flag PEO mutant #2. Western blot analysis was carried out with the indicated antibodies. The relative levels of PolγA to hsp60 have been quantitated from 3 biological replicates. **(B)** PEO mutants undergo the same level of ubiquitylation as PolγA WT in mitochondrial lysates from HeLa shMITOL. (Left) Whole mitochondrial lysates were isolated from HeLa shGFP and HeLa shMITOL cells expressing Flag PolγA WT, Flag PEO mutant #1, and Flag PEO mutant #2. Western blot analysis was carried out with the indicated antibodies. (Center and right) Immunoprecipitations were carried out with anti-Flag antibody (or the corresponding IgG) using whole mitochondrial lysates isolated from HeLa shGFP and HeLa shMITOL cells expressing Flag PolγA WT, Flag PEO mutant #1, and Flag PEO mutant #2. The immunoprecipitates were probed with the indicated antibodies. Three biological replicates were carried out, and the same results were obtained in each case. **(C, D)** Lack of MITOL allows PEO mutants to carry out mtDNA replication. (C) mtDNA replication in HeLa shMITOL cells expressing Flag PolγA WT, Flag PEO mutant #1, and Flag PEO mutant #2 were determined either by (top) Southwestern analysis or (bottom) Slot blot western using anti-BrdU antibody. (Middle) An EtBr gel for NheI digestion of mtDNA shows equal amount of DNA taken for both the assays. (D) Quantification of (C) from 3 biological replicates. Numerical values for all graphs can be found in S1 Data. IgG, immunoglobulin G; mtDNA, mitochondrial DNA; PEO, progressive external ophthalmoplegia; WT, wild-type.

https://doi.org/10.1371/journal.pbio.3001139.g005

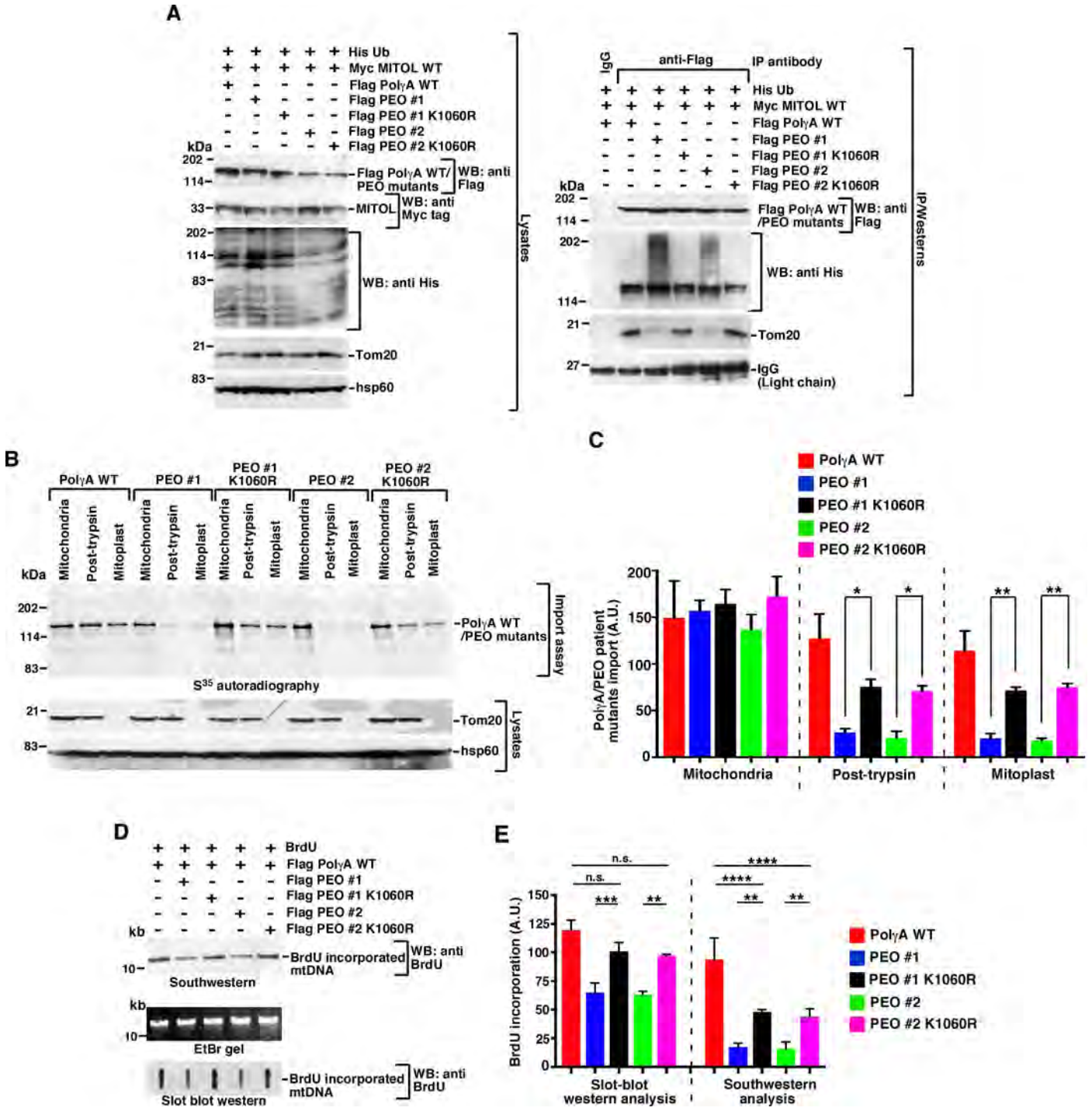

Fig 6. PEO mutants can be reactivated by preventing their ubiquitylation at K1060. (A) A subset of PEO mutants can be reactivated by mutating their site of ubiquitylation by MITOL. (Left) Whole cell extracts were made from HEK293T cells transfected with Myc MITOL WT, Flag PolγA WT, Flag PEO mutant #1, Flag PEO mutant #1 K1060R, Flag PEO mutant #2, and Flag PEO mutant #2 K1060R. Western blot analysis was carried out with the indicated antibodies. (Right) Immunoprecipitations were carried out with anti-Flag antibody (or the corresponding IgG), and the immunoprecipitates were probed with the indicated antibodies. Three independent biological replicates were carried out, and the same result was obtained. **(B, C)** K1060R counterparts of PEO mutants #1 and #2 can enter mitochondria with similar efficiency was PolγA WT. (B) (Top) Mitochondrial import assay was carried out using the indicated mitochondrial fractions. S^{35} methionine radiolabeled Flag PEO mutant #1, Flag PEO mutant #1 K1060R, Flag PEO mutant #2, and Flag PEO mutant #2 K1060R were incubated with each of the mitochondrial fractions. The amount of product in each compartment was detected by autoradiography. (Bottom) The purity of the mitochondrial fractions was determined using the indicated antibodies. (C) Quantification of (B) from 3 biological replicates. **(D, E)** Cells expressing K1060R variant PEO mutants #1 and #2 can be reactivated to incorporate BrdU. (D) mtDNA replication in HEK293T cells expressing Flag PolγA WT, Flag PEO mutant #1, Flag PEO mutant #1 K1060R, Flag

PEO mutant #2, and Flag PEO mutant #2 K1060R were determined either by (top) Southwestern analysis or (bottom) Slot blot western using anti-BrdU antibody. (Middle) An EtBr gel for NheI digestion of mtDNA shows equal amount of DNA taken for the 2 assays. (E) Quantification of (D) from 3 biological replicates. Numerical values for all graphs can be found in S1 Data. See also S6 Fig. His-Ub, His-tagged ubiquitin; IgG, immunoglobulin G; PEO, progressive external ophthalmoplegia; WT, wild type.

https://doi.org/10.1371/journal.pbio.3001139.g006

dynamics and interconnectivity between the mitochondria and endoplasmic reticulum [24,32–34]. Perhaps more importantly, MITOL also acts as a component in the mitochondrial quality control at the OMM by ubiquitylating and degrading diverse toxicity inducing proteins like mutant SOD1, mutant short chain acyl CoA dehydrogenase, mutant MITOL itself and polyglutamine expanded protein, and MAVS aggregates [20–23].

Very recently, it has been shown that MITOL-mediated ubiquitylation of mitochondrial proteins negatively regulates their entry into the organelle [28]. This can be rationalized as mitochondria needs a level of control which allows the entry of these proteins in a regulated and "on demand" manner. We now provide evidence to show that compared to PolγA ubiquitylated by MITOL, non-ubiquitylated PolγA binds better with Tom20, which allows it to enter the mitochondria, and thereby carry out mtDNA replication. Hence, we conclude that the mere presence of MLS is not sufficient for proteins to enter into the mitochondrial matrix, and a finer regulatory control like ubiquitylation is necessary.

Previous reports have suggested that ubiquitylation by MITOL of misfolded proteins and their subsequent elimination from the system is important for optimal mitochondrial homeostasis [20–23]. We now provide evidence that 50% of the examined PEO mutants undergo hyperubiquitylation by MITOL on the OMM, which prevents them from binding to Tom20 receptor with maximum efficiency. Thus, ubiquitylation of these PEO patient-derived PolγA diminishes their entry into the mitochondrial matrix and consequently affects their functions in mitochondrial replication and mtDNA repair. Further, PEO mutants #1 and #2 were present much more in the insoluble fraction compared to their WT counterpart. It is conceivable that these PEO mutants which cannot enter mitochondria possibly have alterations in their respective conformations after MITOL-dependent ubiquitylation, which allows them to become better MITOL targets. In fact, it has been demonstrated that conformation change in microtubule-associated protein 1B light chain 1 (LC1) allowed it to be targeted by MITOL [21].

MITOL has been shown to ubiquitylate its substrates either via K48 or K63 linkages [20,23,26]. Here, we demonstrate that MITOL can ubiquitylate PolγA via noncanonical K6 linkage. Usage of "R" and "O" ubiquitin mutants *in vitro* and K6 affimer *in vivo* provided the experimental evidence for this specific linkage. Interestingly, it has been recently shown that Mitofusin2, which is targeted by MITOL [24], is also targeted by another E3 ligase HUWE1 in a K6-linked manner [27]. K6-linked ubiquitylation linkages accumulate with faster kinetics after proteasomal inhibition [35]. This is possibly due to its reduced rates of USP14-dependent deubiquitylation of K6 linkages due to their structural orientation [36]. However, we provide evidence that PolγA is not a substrate of HUWE1. Instead, PolγA is specifically ubiquitylated by MITOL via K6 linkage.

Evidence exists detailing the biochemical mechanisms by which the various mutant PolγA proteins function [37,38]. It is undeniable that the compromised catalytic activity of PEO mutants play a major role in mtDNA replication defect in these patients. For example, active site PolγA Y955C mutant (PEO mutant #4 in our study) has been shown to have dominant effect leading to less than 1% polymerase activity, decreased processivity, increased error prone DNA synthesis, and stalling phenotypes [2,39,40]. The spacer domain mutation PolγA A467T (PEO mutant #2 in our study) has compromised catalytic efficiency and decreased

polymerase activity, DNA binding, and processivity—effects which have been linked to its lack of optimal interactions with the accessory factor [3]. The most common PolγA mutation W748S (PEO mutant #3 in our study) also show significantly reduced polymerase activity [4]. In this study, the polymerization and exonuclease assays performed using recombinant PolγA WT and PEO mutants have also validated the published biochemical work. Furthermore, structural studies on WT PolγA [25] have validated most of the biochemical published reports. However, it should be noted that the biochemical or structural studies were all carried out with recombinant purified proteins and not in an *in vivo* milieu, only where posttranslational modifications like MITOL-dependent ubiquitylation on PolγA can occur.

Similarly, lack of one to one correlation between the *in vitro* and *in vivo* results has been noticed in some of our other results. For example, while we observe that USP30 deubiquitylates PolγA *in vitro*, its expression in asynchronously growing cells does not rescue MITOL-dependent decrease in the level PolγA nor alter the extent of PolγA ubiquitylation. Based on our data and also the recent literature [28], we believe that *in vivo* USP30 may act as a deubiquitylase to MITOL-ubiquitylated PolγA only under very specific physiological conditions, which needs to be further investigated.

In recent time, efforts are being made to carry out mitochondrial genome engineering using multiple manipulative techniques [41,42]. Ablation of MITOL can allow the 2 PEO mutants #1 and #2 to enter mitoplast and be reactivated. However, removal of MITOL from cellular milieu will have substantial effects on vital cellular functions and will be difficult to implement. Hence, the alternate usage of K1060R derivatives of PEO mutants #1 and #2 will ensure lack of MITOL-specific polyubiquitylation and allow their better binding to Tom20, leading to the reentry of these PolγA variants into mitochondria and become functionally active. It will be interesting to test whether the reactivation of PolγA can actually be carried out *in vivo* using mitochondrial genome editing techniques.

In conclusion, we have deciphered the mechanism by which PolγA enters into the mitochondria to an optimal extent (Fig 7). We show that for a subset of the PolγA mutants, apart from the lack of their optimal catalytic activity, an additional level of regulation exists within the cells which negatively control their mitochondrial entry and thereby their functions inside the mitochondrial matrix. These results complement the current dogma that MLS of Polγ and its interactions with TOM complex are sufficient for its entry into mitochondria. It is interesting to note that under pathological abnormalities like during certain cases of PEO, this fined-tuned mechanism of WT PolγA import is no longer operational. Hence, under these conditions where hyperubiquitylation of PEO mutants occur, the reactivation of PolγA may help in reverting phenotypes associated with mitochondrial disorders and thereby lead to near optimal levels of mtDNA replication.

Materials and methods

Reagents

All the antibodies and recombinant DNAs used are listed in S2 and S3 Tables, respectively. All chemicals, recombinant proteins, cell lines, siRNAs, and kits used are listed in S4 Table. Primers used for different assays are listed in S5 Table.

Plasmids, siRNAs, and RT-qPCR

All mutants listed in S3 Table were generated by site directed mutagenesis. Catalytically dead MITOL (MITOL CD) was generated by incorporating the following changes in the WT amino acid sequence: C65S, C68S, and H43S. GST MITOL WT/CD was generated by sub-cloning MITOL WT sequence at BamH1/XhoI sites in pGEX4T-1. Untagged PolγA, named as pcDNA

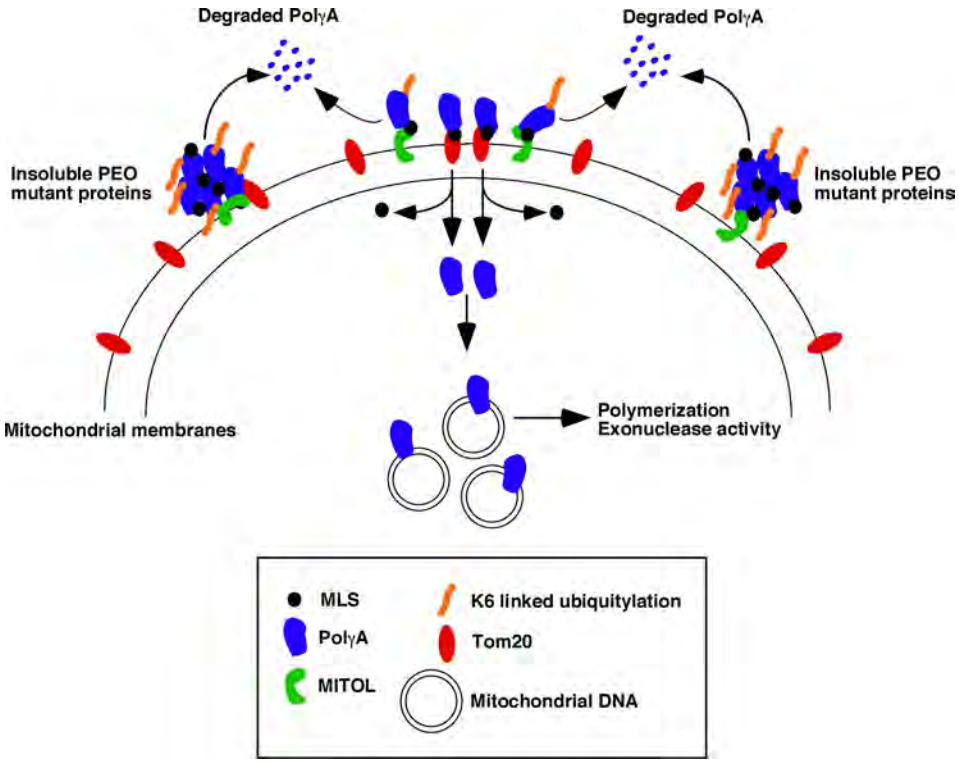

Fig 7. MITOL-dependent ubiquitylation negatively regulates PolγA entry into mitochondria and thereby mtDNA replication. PolγA has a key role in mtDNA replication. WT PolγA is targeted by MITOL, an E3 ligase present in the OMM. MITOL ubiquitylates PolγA at K1060 via K6 linkage. This ubiquitylation event prevents PolγA from efficiently binding to Tom20. Consequently, only non-ubiquitylated PolγA (which binds with Tom20) could enter the mitochondrial matrix, thereby allowing it to do its functions during mtDNA replication. This regulated entry of PolγA into mitochondria is no longer operational under pathological situations. In cells expressing certain PolγA variants present in PEO patients, the mutant PolγA proteins are hyperubiquitylated by MITOL and hence cannot enter into mitochondria. Instead, these proteins are present in the insoluble fraction, which allows them to be recognized and targeted for degradation. Consequently, the lack of entry of the mutated PolγA proteins into mitochondria leads to decreased mtDNA replication and thereby diminished ability to maintain the mitochondrial genome integrity. MLS, mitochondrial localization signal; mtDNA, mitochondrial DNA; PEO, progressive external ophthalmoplegia; PolγA, polymerase γ subunit A; WT, wild-type.

https://doi.org/10.1371/journal.pbio.3001139.g007

3.1 hygro (+) PolγA WT, was generated by sub-cloning PolγA WT sequence at NheI/BamH1 sites in pcDNA 3.1 hygro (+). The siRNA sequences (5′ to 3′) for MITOL were siRNA#1: GCU CUA UCU AUU GGA CAG and siRNA#2: UCU UGG GUG GAA UUG CGU U [43]. The siRNA sequence (5′ to 3′) to HUWE1 was CCC GCA UGA UCU UGA AUU U [44]. RNA isolation for reverse transcription quantitative polymerase chain reaction (RT-qPCR) and its conversion to cDNA were carried out using Trizol reagent (Thermo Fisher Scientific, Waltham, Massachusetts, United States) and Reverse transcriptase core kit (Eurogentec, Liege, Belgium), respectively, according to the manufacturers' protocols. The RT-qPCR reactions were carried out in QuantStudio 3 Real-time PCR system (Thermo Fisher Scientific).

Cell culture treatments and confocal imaging

Both plasmid and siRNA transfections were carried out with Lipofectamine 2000 (Thermo Fisher Scientific) for 6 hours according to manufacturer's protocol. In a 6 well cluster, either 0.25 to 1 μg of the plasmid DNA or 200 pmoles of the respective siRNAs or siControl were used. For all cell culture experiments (except in Fig 4E), lysates were made 24 hours post-transfection. To determine the difference in the rate of ubiquitylation and degradation between WT

and mutant PolγA (as seen in Fig 4E), lysates were made 12 hours post-transfection. This included the period of MG132 (10 μM) treatment which was carried out for 5 hours immediately prior to the preparation of the lysates. CHX (1 mM) treatments were carried out for the indicated time periods. To obtain the soluble and insoluble fractions, the transfected cells were lysed in a lysis buffer (50 mM Tris-HCl pH 7.4, 150 mM NaCl, 5 mM EDTA, 1% Triton X-100, and protease inhibitor cocktail) by pipetting gently and rotating for 10 minutes at 4˚C. Soluble and insoluble fractions were separated by centrifugation at 20,000g for 20 minutes at 4˚C. Immunofluorescence staining was carried out as described [45,46]. All imaging was carried out in LSM 510 Meta System (Carl Zeiss, Germany) with 63×/1.4 oil immersion objective. The laser lines used were Argon 458/477/488/514 nm (for FITC), DPSS 561 nm (for Alexa Fluor 594), and a Chameleon Ultra auto-tunable femtosecond laser 690–1050 nm (for DAPI). All parameters were kept constant during image acquisitions using LSM5 software for particular experiments. Colocalization factor is defined as [(Fraction of cells having colocalization) × (Fraction of foci colocalized per cell)] × 100 [47]. Colocalization factor was calculated for 100 cells spread over 3 independent experiments.

In vitro ubiquitination assay

During *in vitro* ubiquitylation assays, GST MITOL WT/CD (1.6 μM) were incubated with equal amount (2 μl) of S^{35} methionine labeled *in vitro* transcribed and translated PolγA in the ubiquitylation buffer (40 mM Tris-HCl, pH 7.5, 5 mM $MgCl_2$, and 2 mM ATP) in presence of 100 ng E1 (UBE1), 300 ng E2 (UbcH5a), and 2 μM Ubiquitin. MITOL WT/CD (0.8 μM) was added at the end to initiate the reaction. Normally, the ubiquitylation reactions were carried out at 30 ^{o}C for 2 hours. To obtain gradient of PolγA ubiquitylation, the reactions were stopped after 5 minutes or 20 minutes. Post-reaction, samples were boiled with SDS-PAGE sample buffer and subjected to western analysis. It is to be noted that PolγA ubiquitylated smears were not observed upon autoradiography. This was due to the fact that the SDS-PAGE gels had to be subjected to fluorography (as S^{35} Methionine is a weak beta emitter), and the gels dried at 65˚C for 3 to 4 hours, before being exposed for autoradiography. The process of fluorography and/or the heating the gels during the drying process degraded the ubiquitylated products for a high molecular weight substrate like PolγA.

Apart from WT ubiquitin, "R" and "O" ubiquitin mutants have been used in these assays. In "R" ubiquitin mutants, only a particular lysine residue in ubiquitin is mutated, while in "O" ubiquitin mutants, only 1 lysine is present on ubiquitin, and all other 6 lysines are mutated. For all the linkage studies a limiting concentration (250 nM) of WT ubiquitin, "R" and "O" ubiquitin mutants were used.

In vitro deubiquitination assay

The assay was carried out according to [48]. MITOL-dependent ubiquitylation was standardized in a ubiquitylation–deubiquitylation buffer (20 mM Tris-Cl pH 8.0, 0.01% Triton X-100, 1 mM L-glutathione, 0.03% BSA, 5 mM MgCl2, and 2 mM ATP). The ubiquitylation reaction was done for 90 minutes at 30˚C in presence of 100 ng E1 (UBE1), 300 ng (UbcH5a), 2 μM Ubiquitin, and 0.8 μM MITOL. USP30 (0.8 μM) was added either with MITOL (called simultaneous reaction) or after the completion of the MITOL-dependent ubiquitylation (called sequential reaction). For the sequential reaction, the incubation was continued for a further 90 minutes.

Isolation of mitochondria

Mitochondria were isolated from both HEK293T cell lines. For this purpose, 5 to 10 × 10^9 HEK-293T cells were grown as monolayers, washed with 1X PBS, and harvested in

mitochondria isolation buffer (20 mM Hepes, pH 7.5, 1.5 mM $MgCl_2$, 1 mM EDTA, 1 mM EGTA, 210 mM sucrose, and 70 mM mannitol). HEK293T cell suspension was subjected to 60 gentle strokes using Dounce homogenizer. The supernatant obtained was again centrifuged at 10,000Xg for 15 minutes at 4˚C. The resultant mitochondrial pellet was washed twice and suspended in 200 μl buffer containing 250 mM sucrose, 5 mM magnesium acetate, 40 mM potassium acetate, 10 mM sodium succinate, 1 mM DTT, and 20 mM Hepes/KOH, pH 7.4.

In vitro transcription, translation, and import assay

In vitro transcription and translation was carried out with 1 μg of the supercoiled DNA in presence of ^{35}S methionine using T7 Quick Coupled Transcription/translation system. The reaction was done for 90 minutes at 30˚C, following which products were checked by autoradiography in SDS-PAGE. The labeled WT PolγA and PEO mutants were used in import assays as described previously [46]. Six such reactions were set up in parallel with the mitochondria isolated from HEK293T cells. In the first reaction, labeled proteins (2 μl), which have been either ubiquitylated or non-ubiquitylated by MITOL, were incubated with 200 μg of isolated total mitochondria in import buffer (0.25 M sucrose, 1.5 mM $MgCl_2$, 2.5 mg/ml BSA, and 10 mM HEPES, pH 7.2) supplemented with 2 mM ATP, 2 mM GTP, 5 mM Magnesium Acetate, 20 mM KCl, and 2 mM succinate. Reaction was initiated at 37˚C by ATP and lasted for 60 minutes. For this first reaction, one-half of each sample was assessed for the presence of the proteins by western analysis in the total mitochondria, and the other half was kept for autoradiography. For the second reaction, the import assay was carried out as above. Further, the mitochondria were treated with trypsin (final concentration 20 μg/ml) on ice for 15 minutes to remove the outer membrane proteins. After inhibiting trypsin with soybean trypsin inhibitor (final concentration 50 μg/ml), mitochondria were re-isolated by passing it through a sucrose cushion (0.8 M sucrose in 10 mM HEPES, pH 7.2) by centrifuging at 12,000 rpm for 10 minutes (to remove the proteins which have been digested by trypsin treatment). At this stage, half of this second reaction was kept for western and the other half for autoradiography. In the third reaction, the reaction was done as above. Further, the mitoplast was isolated by resuspending the mitochondria in a hypotonic buffer (20 mM KCl and 10 mM HEPES, pH 7.2) or treated with 0.1% digitonin and incubated on ice for 20 minutes. The resulting mitoplasts were re-isolated by centrifugation at 12,000 rpm for 10 minutes and passed through the sucrose cushion to remove the OMM proteins. At this stage of the third reaction, half of the material was kept for western and the other half for autoradiography. In the fourth reaction, after removal of the OMM proteins, the mitochondrial matrix was isolated by resuspending the samples in a hypotonic buffer (5 mM Tris-HCl 7.4 and 1 mM EDTA) and sonicated mildly (2 pulse, 10 seconds each with 10 seconds off between the cycles). Sonicated samples were centrifuged at 40,000 rpm for 45 minutes at 4 ^{o}C. The resultant pellet constituted the inter-mitochondrial membrane (IMM), and supernatant contained the mitochondrial matrix fraction. The supernatant was precipitated using Trichloroacetic acid (TCA) (1 volume of 100% TCA to 4 volumes of supernatant) to concentrate the proteins. Again, the sample were divided in 2 parts—half of this reaction was kept for western and the other half for autoradiography. In fifth reaction, import assay was carried out in presence of 20 μM CCCP to dissipate membrane potential. Further, the mitochondria were treated with trypsin (final concentration 20 μg/ml) on ice for 15 minutes to remove the outer membrane proteins. After inhibiting trypsin with soybean trypsin inhibitor (final concentration 50 μg/ml), mitochondria were re-isolated by passing it through a sucrose cushion (0.8 M sucrose in 10mM HEPES, pH 7.2) by centrifuging at 12,000 rpm for 10 minutes (to remove the proteins which have been digested by trypsin treatment). At this stage, half of this reaction was kept for western and the other half for

autoradiography. In sixth reaction, after import assay, mitochondria were lysed by treatment with 1% Triton X-100 (V/V) before the trypsin treatment. Mitochondria were re-isolated by passing through sucrose cushion. Further samples were divided into two half, one for western blot and the other half for autoradiography.

Protein purification and interaction studies

All proteins in *Escherichia coli* were expressed in BL21-CodonPlus-RP competent cells strain by adding 1 mM of Isopropyl-1-thio-β-D-galactopyranoside (IPTG) and incubating the culture at 200 rpm, 18˚C for 6 hours. The sonication was carried out in Bandelin Sonoplus HD2070 sonicator using a MS73 probe. Cell slurry was made in 1X PBS supplemented with Protease inhibitor cocktail, 1 M phenylmethylsulfonyl fluoride (PMSF, final concentration 1 mM) and 1 M dithiothreitol (DTT, final concentration 1 mM). A minimum of 5 sonication cycles (30 seconds on, 30 seconds off, 50% cycle, and 20% power) was used. Post sonication, Triton X-100 (prepared in 1X PBS) was added to the suspension at a final concentration of 2%. The suspension was kept for mixing in end-to-end rocker for 30 minutes at 4˚C, followed by centrifugation for 30 minutes at 12,000 rpm at 4˚C. Subsequently, the supernatant was bound to glutathione–sepharose resin equilibrated in GST buffer (50 mM Tris-HCl (pH 7.5), 100 mM KCl, 10 mM $MgCl_2$, 5% Glycerol, and 0.5% NP-40). The bound proteins were washed thrice with GST buffer, loaded onto Poly-Prep Chromatography column kept at 4˚C, and eluted by using a stepwise gradient of glutathione (5 mM and 10 mM prepared in GST buffer). The samples from the eluted fractions were checked in a Coomassie stained gel. The fractions containing the pure proteins were pooled and dialysed against the dialysis buffer (25 mM Tris pH 7.5, 140 mM NaCl, 15% Glycerol, and 1 mM DTT) overnight with 2 changes. The dialyzed purified proteins were then quantified, aliquoted in a storage buffer (25% glycerol, 25 mM Tris pH 7.5, and 140 mM NaCl) and stored in −80˚C till further use. To prepare purified proteins in mammalian cells, Flag or Myc-tagged proteins were over expressed in HEK 293T cells for 24 hours. Lysates were prepared from HEK 293T using M2 lysis buffer and expression checked using anti-Flag or anti-Myc tag antibodies. Post-checking, Flag or Myc-tag proteins were immunopurified using either anti-Flag beads or anti-Myc tag antibodies.

For anti-Flag or anti-Myc tag immunoprecipitations, 100 to 200 μg of lysates overexpressing the respective proteins was used, while for endogenous interactions, 500 μg to 1 mg of the mitochondrial extracts were taken. Using anti-Flag beads (1 to 2 μl) or the antigen-specific antibodies (1 to 2 μg), immunoprecipitations were carried out for 4 hours at 4˚C, after which the complexes were washed thrice with the respective lysis buffers at 4˚C. For elution of Flag bound proteins, the protein bound beads were incubated with Flag peptide (final concentration 100 μg/ml) for 1 hour. The supernatant obtained post-centrifugation was checked by western blot analysis and Coomassie. To determine the interacting proteins, the immunoprecipitates were subjected to SDS-PAGE and probed with the corresponding antibodies. For *in vitro/in vivo* PolγA-MITOL interactions, GST-tagged proteins (1 to 2 μg) were incubated with the lysates (100 to 200 μg) overexpressing the corresponding proteins. For interactions between PolγA with GST-MITOL, 1 to 2μl of [^{35}S] Methionine radiolabeled *in vitro* transcribed and translated PolγA was incubated with the bound GST proteins (1 to 2 μg) for 6 hours. The bound radioactivity was detected by autoradiography.

Immunoblotting

For western blotting, lysate was prepared using RIPA buffer [1 mM Tris-HCl pH 7.8, 150 mM NaCl, 2% Triton X-100, 1% (w/v) Sodium deoxycholate, and 0.1% (w/v) SDS supplemented with 1X PIC and 1 mM PMSF]. For western blotting, equal amounts (typically 40 to 50 μg) of

the lysates were run in appropriate percentage of SDS-PAGE gels, transferred to nitrocellulose membranes (usually overnight at 40 mA per gel), and incubated with the respective primary antibodies (listed in S2 Table) overnight at 4˚C with gentle rocking. Next day, the blots were incubated with the respective secondary antibodies for 1 hour and washed and developed using the chemiluminescent detection system.

Primer extension assay

Primer extension assays were carried out according to a published protocol [49,50]. The primer-template pair (S5 Table) comprised of the first 40 nucleotides of the mtDNA replication origin. The annealed substrate (10 μM) was incubated with the indicated amounts of the PolγA/B2 holoenzyme in a buffer containing 10 mM Tris-HCl, pH 7.4, 8 mM MgCl2, 0.1 mM DTT, 100 μg BSA/ml, 50 μM each of dCTP, dGTP, and dTTP, 1 μM dATP, and [α-P^{32}] dATP (0.5μCi). The products were analyzed in a 15% acrylamide-8M urea gel. Primer extension was visualized by the incorporation of [α-P^{32}] dATP due to the polymerization functions of PolγA/B2. The radioactive 40-mer produced was quantitated in a phosphoimager.

Exonuclease assay

Exonuclease assay was carried out as previously described [50,51]. The [γ-^{32}P] ATP labeled 25-mer primer with 4 mismatches at 3′ end was annealed to 45-mer template (S5 Table). Annealed substrate (10 nM) was incubated with the indicated amounts of PolγA in a buffer containing 25 mM HEPES-KOH, pH 7.6, 1 mM βME, 5 mM $MgCl_2$, 0.05 ng/ml BSA, and 10 mM NaCl. The reaction was initiated by adding PolγA and incubated at 37 ^{o}C for 3 minutes. The products were analyzed in a 15% acrylamide-8M urea sequencing gel. Exonuclease activity of PolγA was visualized by the formation of progressively smaller products due to the exonuclease functions of PolγA. All smaller products were quantitated in a phosphoimager.

Slot blot and Southwestern analysis

HEK293T cells were transfected the PolγA variants. After 24 hours, cells were treated with 10 μM BrdU and incubated for another 24 hours. Transfected cells were harvested, and mtDNA was isolated using mtDNA isolation kit (BioVision, Milpitas, California, US), according to manufacturer's protocol. For slot blot analysis, mtDNA (2 μg) were boiled at 100˚C for 10 minutes and transferred directly onto nitrocellulose membrane using slot blot apparatus (Cleaver Scientific, England). For Southwestern analysis, 1 μg of the isolated mtDNA's were digested with NheI restriction enzyme and separated on 1% agarose gel. DNA were transferred onto nitrocellulose membrane using VacuGene XL (GE Healthcare, Chicago, Illinois, US) according to manufacturer's protocol. Post-transfer, membranes obtained were UV cross-linked, blocked with 100% normal horse serum for 1 hour at room temperature, and probed using anti-BrdU antibody to check BrdU incorporation.

Long-range mtDNA amplification assay

A total of 20 ng of mtDNA template was used to amplify mtND1 and full-length mtDNA using LongAmp Taq DNA polymerase using the primers whose sequence is in S5 Table. PCR reactions were performed at 94˚C for 30 seconds followed by 30 cycles at 94˚C for 30 seconds, 65˚C for 14 minutes, and a final elongation for 10 minutes. The products were separated by electrophoresis on a 1% agarose gel stained with ethidium bromide.

Statistical analysis

All data are presented as mean ± SD. * $p < 0.05$, ** $p < 0.01$, *** $p < 0.001$, **** $p < 0.001$, while n.s. indicates that the result is not significant. The statistical analyses employed for every experiment are shown in S6 Table.

Supporting information

S1 Fig. Factors determining the interaction between MITOL and PolγA (related to Fig 1). (A, B) Overexpression and ablation of MITOL does not alter PolγA transcript levels. HEK293T cells were either (A) transfected with either Myc MITOL or the corresponding vector or (B) transfected with either siControl or siMITOL RNA was isolated and RT-qPCR carried out to detect the levels of MITOL and PolγA. The transcript levels of GAPDH was used as control. **(C) Endogenous PolγA colocalize with MITOL.** Asynchronously growing NHFs were stained with antibodies against PolγA and MITOL. DNA was stained by DAPI. Scale, 5 μM. The colocalization factor has been indicated. Representative images are shown. **(D) Overexpressed PolγA colocalize with exogenously expressed MITOL.** U-2 OS cells were transfected with Flag PolγA WT and Myc MITOL. Cells were stained with anti-Flag and anti-Myc tag antibodies. Scale, 5 μM. Representative images are shown. **(E) Spacer and thumb domains of PolγA interacts with MITOL.** (Middle and bottom panels which constitute the input) Myc-MITOL expressed in HEK293T was detected by anti-Myc antibody and bound GST or GST-PolγA proteins [PolγA (53–439), PolγA (440–1239), PolγA (440–815), PolγA (816–1239), and PolγA (53–1239)] were detected by Coomassie staining. (Top) The interactions between Myc-MITOL and bound GST or GST-PolγA proteins were detected with anti-Myc tag antibody. Three independent biological replicates were carried out, and the same result was obtained. **(F) Carboxyl terminus loop of MITOL interacts with PolγA.** (Left panels, which constitute the input) PolγA (as visualized by western analysis of the S^{35} methionine radiolabeled *in vitro* transcribed and translated product with anti-PolγA antibody) and bound GST or GST-MITOL [MITOL (1–278), MITOL (1–191), MITOL (159–210), and MITOL (253–278)] were visualized by Coomassie staining. (Right) Interaction was carried out between S^{35} methionine radiolabeled PolγA and bound GST or GST-MITOL proteins. The amount of radiolabeled PolγA bound to the GST-tagged proteins was detected by autoradiography. Three independent biological replicates were carried out, and the same result was obtained. Numerical values for all graphs can be found in S1 Data. NHF, normal human fibroblast; PolγA, polymerase γ subunit A; RT-qPCR, reverse transcription quantitative polymerase chain reaction; WT, wild-type.
(PDF)

S2 Fig. Factors which indicate the specificity of PolγA as a substrate for MITOL (related to Fig 2). (A) PolγA is not a substrate of HUWE1. Lysates were made from HEK293T cells transfected with either siControl or siHUWEI or siMITOL. Western blot analysis was carried out with the indicated antibodies. Three independent experiments were done, and the same results were obtained. **(B) Coomassie gel showing purified recombinant His GST USP30 and GST MITOL.** Coomassie gels indicating the purity of His GST USP30 and GST-MITOL used in the assays. Three independent protein preparations were used for the experiments. **(C, D) USP30 deubiquitylates PolγA *in vitro*.** *In vitro* ubiquitylation reactions were carried out using PolγA as the substrate and MITOL WT. Recombinant USP30 was added either (C) during the *in vitro* ubiquitylation assay (called simultaneous) or (D) after MITOL-mediated *in vitro* ubiquitylation assay (called sequential). Post-reaction, the products were detected by western blot analysis with the indicated antibodies. Three biological replicates were carried

out, and the same result was obtained. **(E) Overexpression of USP30 cannot revert MITOL-mediated degradation of PolγA.** Lysates were made from HEK293T cells transfected with either Flag USP30 or Myc MITOL WT. Western blot analysis was carried out with the indicated antibodies. Three independent experiments were done, and the same results were obtained. **(F) Overexpression of USP30 cannot revert MITOL-mediated ubiquitylation of PolγA.** Immunoprecipitations with either PolγA antibody (or the corresponding IgG) were carried out with lysates were made from HEK293T cells transfected with either Flag USP30 or Myc MITOL WT. Western blot analysis was carried out with the indicated antibodies. Three independent experiments were done, and the same results were obtained. IgG, immunoglobulin G; PolγA, polymerase γ subunit A; WT, wild-type.
(PDF)

S3 Fig. Catalytically active MTOL can ubiquitylate PolγA via specific linkage (related to Fig 3). (A) Generation of ubiquitylated and non-ubiquitylated PolγA. MITOL WT or CD dependent *in vitro* ubiquitylation reactions were carried out with PolγA WT or K1060R. The ubiquitylated products were detected by carrying out western blot analysis with anti-Ub (P4D1) antibodies. Equal amounts of substrates used in each condition was determined by carrying out westerns with anti-PolγA antibodies. Four independent biological replicates were carried out, and the same result was obtained. **(B) Time course of PolγA ubiquitylation by MITOL.** *In vitro* ubiquitylation reactions were carried out using PolγA as the substrate and MITOL WT as the E3 ligase. (Top) The ubiquitylation reactions were carried out for 5 minutes and 20 minutes. Post-reaction, the products were detected by western blot analysis with anti-PolγA antibody. (Bottom) Pre-reaction, the amount of PolγA protein used in each ubiquitylation reaction was determined by western analysis using anti-PolγA antibodies. Three independent biological replicates were carried out, and the same result was obtained. **(C) PolγA require catalytically active MITOL during *in vitro* ubiquitylation.** *In vitro* ubiquitylation reactions were carried out using S^{35} methionine radiolabeled PolγA as the substrate and MITOL WT or CD as the E3 ligase. Post-ubiquitylation, the products were detected by carrying out western blot analysis with anti-PolγA antibodies. The reaction products where PolγA were ubiquitylated by MITOL WT were designated as Ub PolγA. Alternately, the products obtained when MITOL CD was used were designated as Non Ub PolγA. The amount of PolγA used in each condition was determined by western blotting with antibodies against PolγA. Three independent biological replicates were carried out, and the same result was obtained. **(D) Purity of GST-Tom20.** Coomassie gels indicating the purity of GST and GST-Tom20 used in the assays. Three independent protein preparations were used for the experiments. **(E) PolγA was ubiquitylated by Ub K6O and not by Ub K6R.** Same as (C) except MITOL-dependent ubiquitylation, reactions for PolγA were carried out with 2 ubiquitin variants—Ub K6R or Ub K6O. Three independent biological replicates were carried out, and the same result was obtained. CD, catalytically dead; PolγA, polymerase γ subunit A; WT, wild-type.
(PDF)

S4 Fig. Controls showing specificity of the entry of a subset of PEO mutants into mitochondria (related to Fig 4). (A) Levels of PolγA WT and PEO mutants. *In vitro* transcribed and translated PolγA WT, PEO mutant #1, PEO mutant #2, PEO mutant #3, and PEO mutant #4 were subjected to SDS-PAGE, and the products were detected by autoradiography. Three independent biological replicates were carried out, and the same result was obtained. **(B) PEO patient #4 shows similar extent of mitochondrial import as PolγA WT.** Mitochondrial import assay was carried out using the indicated mitochondrial fractions. S^{35} methionine radiolabeled PolγA WT, PEO mutant #4 were incubated with each of the mitochondrial fractions. (Bottom) The purity of the mitochondrial fractions was determined using the indicated

antibodies. Three independent biological replicates were carried out, and the same result was obtained. **(C) Relative levels of endogenous and exogenous PolγA WT and PEO mutants.** Lysates were made from HEK293T cells transfected with Flag PolγA WT, Flag PEO mutant #1, Flag PEO mutant #2, Flag PEO mutant #3, and Flag PEO mutant #4. Western blot analysis was carried out with the indicated antibodies. The relative levels of PolγA to hsp60 have been quantitated from 3 biological replicates. **(D) PEO patient #4 shows similar extent of ubiquitylation and binding to Tom20 as PolγA WT.** (Left) Whole cell extracts were made from HEK293T cells transfected with His-Ub, Myc MITOL WT, PolγA WT, and PEO mutant #4. Western blot analysis was carried out with the indicated antibodies. (Right) Immunoprecipitations were carried out with anti-Flag antibody (or the corresponding IgG), and the immunoprecipitates were probed with the indicated antibodies. Three independent biological replicates were carried out, and the same result was obtained. Numerical values for all graphs can be found in S1 Data. His-Ub, His-tagged ubiquitin; IgG, immunoglobulin G; PEO, progressive external ophthalmoplegia; PolγA, polymerase γ subunit A; WT, wild-type.
(PDF)

S5 Fig. Effect of PEO mutants during PolγA-mediated in vitro polymerase and in vitro exonuclease activities (related to Fig 5). (A) Purity of proteins used in primer extension and exonuclease assays. Coomassie gels indicating the purity of GST-tagged PolγA WT, PEO mutant #1, PEO mutant #2, PEO mutant #3, PEO mutant #4, and GST-PolγB used in the primer extension and exonuclease assays. Two independent protein preparations were used for the experiments. (B, C) All PEO mutants show compromised *in vitro* polymerase activity. (B) *In vitro* primer extension assays were carried out with PolγA WT, PEO mutant #1, PEO mutant #2, PEO mutant #3, and PEO mutant #4 using the primer-template pair in presence of [α-P^{32}] dATP. (C) The 40-bp radiolabeled product was quantitated from 3 biological replicates. (D, E) Except PEO mutant #4, all other PEO mutants show compromised *in vitro* exonuclease activity. (D) *In vitro* exonuclease assays were carried out with PolγA WT, PEO mutant #1, PEO mutant #2, PEO mutant #3, and PEO mutant #4 using the [γ-^{32}P] ATP labeled primer annealed to the template. (E) The smaller products obtained were quantitated from 3 biological replicates. Numerical values for all graphs can be found in S1 Data. PEO, progressive external ophthalmoplegia; PolγA, polymerase γ subunit A; WT, wild-type.
(PDF)

S6 Fig. Factors discriminating the entry of PEO mutants into mitochondria (related to Figs 4 and 6). (A, B) Cells expressing PEO mutant #1 and #2 have lower mtDNA integrity. (A) mtDNA integrity was measured using a long-range mtDNA amplification assay in HEK293T cells expressing Flag PolγA WT, Flag PEO mutant #1, and Flag PEO mutant #2. Amplification of mtND1 was used as a control. (B) Quantitation of (A), done with data from 3 biological replicates. **(C, D) Subsets of PEO mutants are present in the insoluble fraction.** (C) Soluble and insoluble fractions were made from HEK293T cells overexpressing Flag PolγA WT, Flag PEO mutant #1, Flag PEO mutant #2, Flag PEO mutant #3, and Flag PEO mutant #4. Western blot analysis was carried out with the indicated antibodies. Equal amounts of the soluble and insoluble fractions were visualized by Coomassie staining. (D) Quantitation of (C), done with data from 3 biological replicates. **(E, F) K1060R mutation in PEO mutants #1 and #2 leads to their decreased presence in the insoluble fraction**. (E) Soluble and insoluble fractions were made from HEK293T cells overexpressing Flag PEO mutant #1, Flag PEO mutant #1 K1060R, Flag PEO mutant #2, and Flag PEO mutant #2 K1060R. Western blot analysis was carried out with the indicated antibodies. (F) Quantitation of (E), done with data from 3 biological replicates. Numerical values for all graphs can be found in S1 Data. mtDNA, mitochondrial DNA; PEO, progressive external ophthalmoplegia; PolγA, polymerase γ subunit

A; WT, wild-type.
(PDF)

S1 Table. Details of patient mutations used in the study.
(PDF)

S2 Table. List of antibodies used in the study.
(PDF)

S3 Table. List of recombinant DNAs used in the study.
(PDF)

S4 Table. List of reagents used in the study.
(PDF)

S5 Table. List of primers used in the study.
(PDF)

S6 Table. Statistical analysis performed in this study.
(PDF)

S1 Data. Numerical raw data. All numerical raw data are combined in a single PDF file, "S1_Data." The presented data underlays Figs 1ACDEFGI, 3BDFHI, 4BEG, 5AD, and 6CE and S1AB, S4C, S5CE, and S6BDF Figs.
(PDF)

S1 Original Images. Original gel and images contained in this manuscript, related to Figs 1ABCDEFGHJ, 2ABCDEFG, 3ACEGHI, 4ACDEF, 5ABC, and 6ABD and S1ADEF, S2ABCDEF, S3ABCDE, S4ABCD, S5ABD, and S6ACE Figs.
(PDF)

Acknowledgments

The authors acknowledge Shigeru Yanagi (Tokyo University of Pharmacy and Life Sciences, Japan), Quan Chen (State Key Laboratory of Membrane Biology, China), Akhil Banerjea, (National Institute of Immunology, India), and Daisuke Kohda (Kyushu University, Japan) for recombinants and Shigeru Yanagi (Tokyo University of Pharmacy and Life Sciences, Japan) for cells and MITOL antibody.

Author Contributions

Conceptualization: Sagar Sengupta.

Data curation: Mansoor Hussain, Aftab Mohammed, Shabnam Saifi, Aamir Khan, Ekjot Kaur, Swati Priya, Himanshi Agarwal.

Formal analysis: Mansoor Hussain, Sagar Sengupta.

Funding acquisition: Sagar Sengupta.

Investigation: Mansoor Hussain, Aftab Mohammed, Shabnam Saifi, Aamir Khan, Ekjot Kaur, Swati Priya, Himanshi Agarwal.

Methodology: Mansoor Hussain, Aftab Mohammed, Shabnam Saifi, Aamir Khan, Ekjot Kaur, Swati Priya, Himanshi Agarwal.

Project administration: Sagar Sengupta.

Resources: Sagar Sengupta.

Supervision: Sagar Sengupta.

Validation: Mansoor Hussain, Aftab Mohammed, Shabnam Saifi, Aamir Khan, Ekjot Kaur, Swati Priya, Himanshi Agarwal.

Visualization: Sagar Sengupta.

Writing – original draft: Sagar Sengupta.

Writing – review & editing: Sagar Sengupta.

References

1. Yakubovskaya E, Chen Z, Carrodeguas JA, Kisker C, Bogenhagen DF. Functional human mitochondrial DNA polymerase gamma forms a heterotrimer. J Biol Chem. 2006; 281(1):374–82. Epub 2005/11/03. https://doi.org/10.1074/jbc.M509730200 [pii] PMID: 16263719.
2. Atanassova N, Fuste JM, Wanrooij S, Macao B, Goffart S, Backstrom S, et al. Sequence-specific stalling of DNA polymerase gamma and the effects of mutations causing progressive ophthalmoplegia. Hum Mol Genet. 2011; 20(6):1212–23. Epub 2011/01/14. https://doi.org/10.1093/hmg/ddq565 PMID: 21228000.
3. Chan SS, Longley MJ, Copeland WC. The common A467T mutation in the human mitochondrial DNA polymerase (POLG) compromises catalytic efficiency and interaction with the accessory subunit. J Biol Chem. 2005; 280(36):31341–6. Epub 2005/07/19. https://doi.org/10.1074/jbc.M506762200 PMID: 16024923.
4. Chan SS, Longley MJ, Copeland WC. Modulation of the W748S mutation in DNA polymerase gamma by the E1143G polymorphismin mitochondrial disorders. Hum Mol Genet. 2006; 15(23):3473–83. Epub 2006/11/08. https://doi.org/10.1093/hmg/ddl424 PMID: 17088268; PubMed Central PMCID: PMC1780027.
5. Ropp PA, Copeland WC. Cloning and characterization of the human mitochondrial DNA polymerase, DNA polymerase gamma. Genomics. 1996; 36(3):449–58. Epub 1996/09/15. https://doi.org/10.1006/geno.1996.0490 PMID: 8884268.
6. Roos S, Macao B, Fuste JM, Lindberg C, Jemt E, Holme E, et al. Subnormal levels of POLgammaA cause inefficient initiation of light-strand DNA synthesis and lead to mitochondrial DNA deletions and progressive external ophthalmoplegia. Hum Mol Genet. 2013; 22(12):2411–22. Epub 2013/03/01. https://doi.org/10.1093/hmg/ddt094 PMID: 23446635.
7. Wiedemann N, Pfanner N. Mitochondrial Machineries for Protein Import and Assembly. Annu Rev Biochem. 2017; 86:685–714. Epub 2017/03/17. https://doi.org/10.1146/annurev-biochem-060815-014352 PMID: 28301740.
8. Bragoszewski P, Turek M, Chacinska A. Control of mitochondrial biogenesis and function by the ubiquitin-proteasome system. Open Biol. 2017; 7(4). Epub 2017/04/28. https://doi.org/10.1098/rsob.170007 PMID: 28446709; PubMed Central PMCID: PMC5413908.
9. Escobar-Henriques M, Langer T. Dynamic survey of mitochondria by ubiquitin. EMBO Rep. 2014; 15(3):231–43. Epub 2014/02/27. https://doi.org/10.1002/embr.201338225 PMID: 24569520; PubMed Central PMCID: PMC3989689.
10. Livnat-Levanon N, Glickman MH. Ubiquitin-proteasome system and mitochondria—reciprocity. Biochim Biophys Acta. 2011; 1809(2):80–7. Epub 2010/08/03. https://doi.org/10.1016/j.bbagrm.2010.07.005 PMID: 20674813.
11. Sickmann A, Reinders J, Wagner Y, Joppich C, Zahedi R, Meyer HE, et al. The proteome of Saccharomyces cerevisiae mitochondria. Proc Natl Acad Sci U S A. 2003; 100(23):13207–12. Epub 2003/10/25. https://doi.org/10.1073/pnas.2135385100 PMID: 14576278; PubMed Central PMCID: PMC263752.
12. Altmann K, Westermann B. Role of essential genes in mitochondrial morphogenesis in Saccharomyces cerevisiae. Mol Biol Cell. 2005; 16(11):5410–7. Epub 2005/09/02. https://doi.org/10.1091/mbc.e05-07-0678 PMID: 16135527; PubMed Central PMCID: PMC1266436.
13. Margineantu DH, Emerson CB, Diaz D, Hockenbery DM. Hsp90 inhibition decreases mitochondrial protein turnover. PLoS ONE. 2007; 2(10):e1066. Epub 2007/10/25. https://doi.org/10.1371/journal.pone.0001066 PMID: 17957250; PubMed Central PMCID: PMC2031825.
14. Radke S, Chander H, Schafer P, Meiss G, Kruger R, Schulz JB, et al. Mitochondrial protein quality control by the proteasome involves ubiquitination and the protease Omi. J Biol Chem. 2008; 283

(19):12681–5. Epub 2008/03/26. https://doi.org/10.1074/jbc.C800036200 PMID: 18362145; PubMed Central PMCID: PMC2442309.

15. Azzu V, Brand MD. Degradation of an intramitochondrial protein by the cytosolic proteasome. J Cell Sci. 2010; 123(Pt 4):578–85. Epub 2010/01/28. https://doi.org/10.1242/jcs.060004 PMID: 20103532; PubMed Central PMCID: PMC2818195.

16. Metzger MB, Scales JL, Dunklebarger MF, Loncarek J, Weissman AM. A protein quality control pathway at the mitochondrial outer membrane. Elife. 2020; 9. Epub 2020/03/03. https://doi.org/10.7554/eLife.51065 PMID: 32118579.

17. Kowalski L, Bragoszewski P, Khmelinskii A, Glow E, Knop M, Chacinska A. Determinants of the cytosolic turnover of mitochondrial intermembrane space proteins. BMC Biol. 2018; 16(1):66. Epub 2018/06/23. https://doi.org/10.1186/s12915-018-0536-1 PMID: 29929515; PubMed Central PMCID: PMC6013907.

18. Chen Z, Liu L, Cheng Q, Li Y, Wu H, Zhang W, et al. Mitochondrial E3 ligase MARCH5 regulates FUNDC1 to fine-tune hypoxic mitophagy. EMBO Rep. 2017; 18(3):495–509. Epub 2017/01/21. https://doi.org/10.15252/embr.201643309 PMID: 28104734; PubMed Central PMCID: PMC5331199.

19. Yonashiro R, Kimijima Y, Shimura T, Kawaguchi K, Fukuda T, Inatome R, et al. Mitochondrial ubiquitin ligase MITOL blocks S-nitrosylated MAP1B-light chain 1-mediated mitochondrial dysfunction and neuronal cell death. Proc Natl Acad Sci U S A. 2012; 109(7):2382–7. Epub 2012/02/07. https://doi.org/10.1073/pnas.1114985109 PMID: 22308378; PubMed Central PMCID: PMC3289331.

20. Sugiura A, Yonashiro R, Fukuda T, Matsushita N, Nagashima S, Inatome R, et al. A mitochondrial ubiquitin ligase MITOL controls cell toxicity of polyglutamine-expanded protein. Mitochondrion. 2011; 11(1):139–46. Epub 2010/09/21. https://doi.org/10.1016/j.mito.2010.09.001 PMID: 20851218.

21. Yonashiro R, Sugiura A, Miyachi M, Fukuda T, Matsushita N, Inatome R, et al. Mitochondrial ubiquitin ligase MITOL ubiquitinates mutant SOD1 and attenuates mutant SOD1-induced reactive oxygen species generation. Mol Biol Cell. 2009; 20(21):4524–30. https://doi.org/10.1091/mbc.e09-02-0112 PMID: 19741096; PubMed Central PMCID: PMC2770940.

22. Kim SH, Park YY, Yoo YS, Cho H. Self-clearance mechanism of mitochondrial E3 ligase MARCH5 contributes to mitochondria quality control. FEBS J. 2016; 283(2):294–304. Epub 2015/10/18. https://doi.org/10.1111/febs.13568 PMID: 26476016.

23. Yoo YS, Park YY, Kim JH, Cho H, Kim SH, Lee HS, et al. The mitochondrial ubiquitin ligase MARCH5 resolves MAVS aggregates during antiviral signalling. Nat Commun. 2015; 6:7910. Epub 2015/08/08. https://doi.org/10.1038/ncomms8910 PMID: 26246171; PubMed Central PMCID: PMC4918326.

24. Sugiura A, Nagashima S, Tokuyama T, Amo T, Matsuki Y, Ishido S, et al. MITOL regulates endoplasmic reticulum-mitochondria contacts via Mitofusin2. Mol Cell. 2013; 51(1):20–34. https://doi.org/10.1016/j.molcel.2013.04.023 PMID: 23727017.

25. Lee YS, Kennedy WD, Yin YW. Structural insight into processive human mitochondrial DNA synthesis and disease-related polymerase mutations. Cell. 2009; 139(2):312–24. Epub 2009/10/20. S0092-8674(09)01044-7 [pii] https://doi.org/10.1016/j.cell.2009.07.050 PMID: 19837034.

26. Shi HX, Liu X, Wang Q, Tang PP, Liu XY, Shan YF, et al. Mitochondrial ubiquitin ligase MARCH5 promotes TLR7 signaling by attenuating TANK action. PLoS Pathog. 2011; 7(5):e1002057. Epub 2011/06/01. https://doi.org/10.1371/journal.ppat.1002057 PMID: 21625535; PubMed Central PMCID: PMC3098239.

27. Michel MA, Swatek KN, Hospenthal MK, Komander D. Ubiquitin Linkage-Specific Affimers Reveal Insights into K6-Linked Ubiquitin Signaling. Mol Cell. 2017; 68(1):233–46 e5. Epub 2017/09/26. https://doi.org/10.1016/j.molcel.2017.08.020 PMID: 28943312; PubMed Central PMCID: PMC5640506.

28. Phu L, Rose CM, Tea JS, Wall CE, Verschueren E, Cheung TK, et al. Dynamic Regulation of Mitochondrial Import by the Ubiquitin System. Mol Cell. 2020; 77(5):1107–23 e10. Epub 2020/03/07. https://doi.org/10.1016/j.molcel.2020.02.012 PMID: 32142684.

29. Ordureau A, Paulo JA, Zhang J, An H, Swatek KN, Cannon JR, et al. Global Landscape and Dynamics of Parkin and USP30-Dependent Ubiquitylomes in iNeurons during Mitophagic Signaling. Mol Cell. 2020; 77(5):1124–42 e10. Epub 2020/03/07. https://doi.org/10.1016/j.molcel.2019.11.013 PMID: 32142685; PubMed Central PMCID: PMC7098486.

30. Kasahara T, Ishiwata M, Kakiuchi C, Fuke S, Iwata N, Ozaki N, et al. Enrichment of deleterious variants of mitochondrial DNA polymerase gene (POLG1) in bipolar disorder. Psychiatry Clin Neurosci. 2017; 71(8):518–29. Epub 2016/12/18. https://doi.org/10.1111/pcn.12496 PMID: 27987238.

31. Shiiba I, Takeda K, Nagashima S, Yanagi S. Overview of Mitochondrial E3 Ubiquitin Ligase MITOL/MARCH5 from Molecular Mechanisms to Diseases. Int J Mol Sci. 2020; 21(11). Epub 2020/05/31. https://doi.org/10.3390/ijms21113781 PMID: 32471110; PubMed Central PMCID: PMC7312067.

32. Karbowski M, Neutzner A, Youle RJ. The mitochondrial E3 ubiquitin ligase MARCH5 is required for Drp1 dependent mitochondrial division. J Cell Biol. 2007; 178(1):71–84. Epub 2007/07/04. https://doi.org/10.1083/jcb.200611064 PMID: 17606867; PubMed Central PMCID: PMC2064424.

33. Nakamura N, Kimura Y, Tokuda M, Honda S, Hirose S. MARCH-V is a novel mitofusin 2- and Drp1-binding protein able to change mitochondrial morphology. EMBO Rep. 2006; 7(10):1019–22. https://doi.org/10.1038/sj.embor.7400790 PMID: 16936636; PubMed Central PMCID: PMC1618377.

34. Park YY, Cho H. Mitofusin 1 is degraded at G2/M phase through ubiquitylation by MARCH5. Cell Div. 2012; 7(1):25. Epub 2012/12/21. https://doi.org/10.1186/1747-1028-7-25 PMID: 23253261; PubMed Central PMCID: PMC3542011.

35. Dammer EB, Na CH, Xu P, Seyfried NT, Duong DM, Cheng D, et al. Polyubiquitin linkage profiles in three models of proteolytic stress suggest the etiology of Alzheimer disease. J Biol Chem. 2011; 286 (12):10457–65. Epub 2011/02/01. https://doi.org/10.1074/jbc.M110.149633 PMID: 21278249; PubMed Central PMCID: PMC3060499.

36. Lee BH, Lu Y, Prado MA, Shi Y, Tian G, Sun S, et al. USP14 deubiquitinates proteasome-bound substrates that are ubiquitinated at multiple sites. Nature. 2016; 532(7599):398–401. Epub 2016/04/14. https://doi.org/10.1038/nature17433 PMID: 27074503; PubMed Central PMCID: PMC4844788.

37. Chan SS, Copeland WC. DNA polymerase gamma and mitochondrial disease: understanding the consequence of POLG mutations. Biochim Biophys Acta. 2009; 1787(5):312–9. https://doi.org/10.1016/j.bbabio.2008.10.007 PubMed Central PMCID: PMC2742478. PMID: 19010300

38. Stumpf JD, Saneto RP, Copeland WC. Clinical and molecular features of POLG-related mitochondrial disease. Cold Spring Harb Perspect Biol. 2013; 5(4):a011395. Epub 2013/04/03. https://doi.org/10.1101/cshperspect.a011395 PMID: 23545419; PubMed Central PMCID: PMC3683902.

39. Graziewicz MA, Longley MJ, Bienstock RJ, Zeviani M, Copeland WC. Structure-function defects of human mitochondrial DNA polymerase in autosomal dominant progressive external ophthalmoplegia. Nat Struct Mol Biol. 2004; 11(8):770–6. Epub 2004/07/20. https://doi.org/10.1038/nsmb805 PMID: 15258572.

40. Ponamarev MV, Longley MJ, Nguyen D, Kunkel TA, Copeland WC. Active site mutation in DNA polymerase gamma associated with progressive external ophthalmoplegia causes error-prone DNA synthesis. J Biol Chem. 2002; 277(18):15225–8. Epub 2002/03/19. https://doi.org/10.1074/jbc.C200100200 PMID: 11897778.

41. Gammage PA, Viscomi C, Simard ML, Costa ASH, Gaude E, Powell CA, et al. Genome editing in mitochondria corrects a pathogenic mtDNA mutation in vivo. Nat Med. 2018. Epub 2018/09/27. https://doi.org/10.1038/s41591-018-0165-9 PMID: 30250142.

42. Jo A, Ham S, Lee GH, Lee YI, Kim S, Lee YS, et al. Efficient Mitochondrial Genome Editing by CRISPR/Cas9. Biomed Res Int. 2015; 2015:305716. Epub 2015/10/09. https://doi.org/10.1155/2015/305716 PMID: 26448933; PubMed Central PMCID: PMC4581504.

43. Yonashiro R, Ishido S, Kyo S, Fukuda T, Goto E, Matsuki Y, et al. A novel mitochondrial ubiquitin ligase plays a critical role in mitochondrial dynamics. EMBO J. 2006; 25(15):3618–26. https://doi.org/10.1038/sj.emboj.7601249 PMID: 16874301; PubMed Central PMCID: PMC1538564.

44. Peter S, Bultinck J, Myant K, Jaenicke LA, Walz S, Muller J, et al. Tumor cell-specific inhibition of MYC function using small molecule inhibitors of the HUWE1 ubiquitin ligase. EMBO Mol Med. 2014; 6 (12):1525–41. Epub 2014/09/26. https://doi.org/10.15252/emmm.201403927 PMID: 25253726; PubMed Central PMCID: PMC4287973.

45. De S, Kumari J, Mudgal R, Modi P, Gupta S, Futami K, et al. RECQL4 is essential for the transport of p53 to mitochondria in normal human cells in the absence of exogenous stress. J Cell Sci. 2012; 125(Pt 10):2509–22. Epub 2012/02/24. https://doi.org/10.1242/jcs.101501 [pii] PMID: 22357944.

46. Kumari J, Hussain M, De S, Chandra S, Modi P, Tikoo S, et al. Mitochondrial functions of RECQL4 are required for the prevention of aerobic glycolysis-dependent cell invasion. J Cell Sci. 2016; 129(7):1312–8. https://doi.org/10.1242/jcs.181297 PMID: 26906415.

47. Sengupta S, Robles AI, Linke SP, Sinogeeva NI, Zhang R, Pedeux R, et al. Functional interaction between BLM helicase and 53BP1 in a Chk1-mediated pathway during S-phase arrest. J Cell Biol. 2004; 166(6):801–13. https://doi.org/10.1083/jcb.200405128 PMID: 15364958.

48. Rusilowicz-Jones EV, Jardine J, Kallinos A, Pinto-Fernandez A, Guenther F, Giurrandino M, et al. USP30 sets a trigger threshold for PINK1-PARKIN amplification of mitochondrial ubiquitylation. Life Sci Alliance. 2020; 3(8). Epub 2020/07/09. https://doi.org/10.26508/lsa.202000768 PMID: 32636217; PubMed Central PMCID: PMC7362391.

49. Achanta G, Sasaki R, Feng L, Carew JS, Lu W, Pelicano H, et al. Novel role of p53 in maintaining mitochondrial genetic stability through interaction with DNA Pol gamma. EMBO J. 2005; 24(19):3482–92. Epub 2005/09/16. 7600819 [pii] https://doi.org/10.1038/sj.emboj.7600819 PMID: 16163384; PubMed Central PMCID: PMC1276176.

50. Gupta S, De S, Srivastava V, Hussain M, Kumari J, Muniyappa K, et al. RECQL4 and p53 potentiate the activity of polymerase gamma and maintain the integrity of the human mitochondrial genome. Carcinogenesis. 2014; 35(1):34–45. Epub 2013/09/27. bgt315 [pii] https://doi.org/10.1093/carcin/bgt315 PMID: 24067899.

51. Johnson AA, Johnson KA. Exonuclease proofreading by human mitochondrial DNA polymerase. J Biol Chem. 2001; 276(41):38097–107. Epub 2001/07/31. https://doi.org/10.1074/jbc.M106046200 [pii]. PMID: 11477094.